Spring 2019

Equilibrium Structures and Thermal Fluctuations in Interacting Monolayers

Emmanuel Rivera
err31@zips.uakron.edu

EQUILIBRIUM CONFIGURATIONS AND THERMAL FLUCTUATIONS IN INTERACTING MONOLAYERS

A Thesis

Presented to

The Graduate Faculty of The University of Akron

In Partial Fulfillment

of the Requirements for the Degree

Master of Science

Emmanuel R Rivera

May, 2019

EQUILIBRIUM CONFIGURATIONS AND THERMAL FLUCTUATIONS IN INTERACTING MONOLAYERS

Emmanuel R Rivera

Thesis

Approved:

Advisor
Dr. J. Patrick Wilber

Faculty Reader
Dr. Malena Español

Faculty Reader
Dr. Dmitry Golovaty

Department Chair
Dr. Kevin Kreider

Accepted:

Dean of the College
Dr. Linda Subich

Dean of the Graduate School
Dr. Chand Midha

Date

ABSTRACT

Coherency strains appear in interacting atomic monolayers due to differing bond lengths, which can arise from different materials or geometries. Examples include extended monolayers interacting with a substrate and the interacting walls of a multi-walled carbon nanotube. These strains can induce various equilibrium configurations, which we will analyze by means of a phenomenological model that incorporates forces from bond stretching and bending within each layer and the weak van der Waals interactions connecting the separate layers. We vary the strengths of each interaction to explore their effects on equilibrium structures, and the specific case of a two-walled carbon nanotube is explored as well. Then, thermal effects are also examined by augmenting the equations with a Langevin model. Finally, indentation simulations, simulations with a hole in the bottom layer with a constant force applied to a section of the top layer, are executed. Simulation results are presented and analyzed.

Thanks to Dr. J. Patrick Wilber, Dr. Malena Español, and Dr. Dmitry Golovaty for guiding me through the entire thesis process and pushing me to go above and beyond the expectations. Thanks to family and friends that supported me through all the stresses of completing a Master of Science in Applied Mathematics.

TABLE OF CONTENTS

LIST OF TABLES

LIST OF FIGURES

CHAPTER I

INTRODUCTION

The use of Molecular Dynamics for the study and design of nanostructures has been extensive. Nanostructures have been shown to have impressive mechanical and electrical properties. Designing nanostructures involves an in-depth analysis of the different physical and chemical properties of the atoms that make up the nanostructure. Below we discuss how atoms in a nanostructure interact with other atoms in the nanostructure and with the environment. Once we have a grasp of what that incapsulates, we briefly describe our mathematical model which is based in part on these interactions between atoms. Once this basic model has been developed, we briefly describe how we incorporate temperature into the model. At the end of this chapter, we summarize our main results.

1.1 Nanostructures

The study of how to fabricate different nanostructures and the study of the properties of these nanostructures has become a large field of inquiry. A few examples of nanostructures are wires, layers, and clusters. Nanowires are one dimensional structures where both the height and width of the structure are measured in nanometers and the length may vary. Nanolayers are two dimensional sheets in which the

thickness is measured in nanometers and the length and width may vary. Nanoclusters are considered to be zero dimensional structures, or those in which all three dimensions are measured in nanometers.[1] All other structures can be constructed from these three main structures. The nanostructures of interest for this thesis are nanotubes and graphene sheets or layers. The structure of a nanotube can be visualized by imagining a graphene layer and rolling it into the shape of an elongated cylinder.[2]

Along with the different forms of nanostructures, they are also made of various materials or chemical compositions. Some examples of this are iron oxide, zinc oxide, and tin dioxide.[3, 4] Structures made from zinc oxide have been shown to aid in the process of removing toxic pollutants in water sources.[5] The structures that motivate our study are typically made from carbon, which is the most extensively studied material for nanostructures. Carbon nanotubes were discovered in 1991 and since then, many varying shapes and materials have been used in the creation of different nanostructures.[6]

As mentioned above, the structure of carbon nanotubes can be visualized in terms of graphene, or the individual nanolayers of graphite. Graphene is one of the thinnest, yet strongest materials known. It has been shown to conduct electricity efficiently and even outperform all other materials as a heat conductor. Carbon nanotubes can be thought of as rolled graphene, while wrapping graphene into a spherical shape creates zero dimensional structures known as fullerenes.[7] Graphene is acquired by means of chemically or mechanically removing it from crystalline graphite

or through direct synthesis by means of chemical vapor deposition with gases that contain carbon.[8]

Bilayer graphene can be considered as a different material from monolayer graphene, even though it is logical to think otherwise.[9] It is believed that the synthesis of graphene by means of standard methods, such as chemical vapor deposition, is self-limiting and will only allow for a single monolayer to be developed; so other methods need to be used to avoid the issue of self-limitation.[10] This adds to the difficulty of fabricating bilayer graphene. There exist different forms of stacking that result when bilayer graphene is synthesized, each form possessing different properties. Two basic types of stackings, AB and AA stacking. AB stacking is where half of the atoms in the top layer lie above atoms in the lower layer and the other half do not while AA stacking has all atoms in the top layer above atoms in the bottom layer. These different stackings possess different electronic structures, absorption spectra, and Coulomb excitations.[11] One advantage of bilayer graphene is that it is the first semiconductor that has a variable band gap, which allows for many new applications.[12]

One of the methods of directly synthesizing graphene is by chemical vapor deposition (CVD). This process requires a substrate on which to develop the graphene. Substrates made of transition metals, such as copper, are used in the synthesis of graphene.[13] As mentioned previously, bilayer graphene requires different methods to develop. One method uses thermal CVD, but with slower cooling rates or by careful manipulation of the substrate.[14] Other methods use higher partial pressure

for deposition in hot wall reactors, or with cold wall CVD with sufficient growth time, both requiring a substrate.[10] Since graphene being synthesized on a substrate is a popular methodology, we wish to explore potential issues in the shape of a developing layer of graphene.

1.2 Physical Properties and Applications

Nanostructures have been shown to have outstanding electrical, thermal, and mechanical properties.[15] Nanostructures have also been shown to have chemical, catalytic, optical, and luminescence properties that are vastly different from larger structures made of the same material.[6] The electrical propagation along carbon nanotubes has been studied as, although they naturally have electrical properties, constructing these nanotubes differently also provides them with other varying electrical properties.[16]

One mechanical property carbon nanotubes have been shown to have is high tensile strength. Single-walled carbon nanotubes can have a critical tensile strength of over 120 GPa, while a bundle of two single-walled carbon nanotubes can have a tensile strength around 80 GPa.[17] At room temperature, the bending rigidity of graphene converges to 2.7 eV. Under certain conditions, the bending rigidity of a carbon nanotube has also been shown to increase with both temperature or the radius of the nanotube.[18]

Due to the variety of their shapes and constituent materials, nanostructures have many possible applications. The creation of DNA like structures and the ability

for miRNA detection of cancerous cells with high sensitivity and good specificity are two examples of nanostructures being used with DNA.[19, 20] In the field of medicine, nanostructures have been used for the delivery of drugs and the binding to cancer cells.[21] Researchers have also explored the use of multishelled hollow carbon nanospheres as an anode in batteries, an application that is possible because of the nanospheres' electrochemical performance and reversible capacity.[22]

1.3 Atomistic Modeling

Atomistic modeling is the construction of a model that is based on the positions of discrete, individual atoms and their interactions with other atoms. This differs from continuum modeling, a basic idea of which is that the material of a body is at every point in the body, so that fields can be defined pointwise. Hence, in a continuum model, positions of individual atoms and interactions between individual atoms are not tracked. We use atomistic modeling as we are looking for details at the microscopic level and it allows us to see the effects of forces on specific atoms. Our approach to create our atomistic model is by means of Molecular Dynamics.

A goal of Molecular Dynamics is to understand the properties of matter starting from the properties of molecules, how they are structured and the microscopic interactions between them. Molecular Dynamics models typically take the form of large systems of differential equations. A key feature is to program computers to efficiently and accurately solve these large systems. These simulations allow us to bridge the microscopic length and time scales with the macroscopic world of a laboratory.

Essentially, we can get macroscopic results by simulating the smaller elements, the individual molecules. However, the accuracy of these macroscopic results is limited by computer memory and precision.

The other way that these simulations can be used as a bridge between the microscopic and the macroscopic is by the comparison of experimental data and a theoretical model. By running simulations based on the theoretical model and comparing the results of that model with the results of experiments, we can determine whether the model is valid.[23]

1.4 Summary of Our Modeling and Results

We will be conducting an atomistic modeling study of equilibrium structures resulting from unidirectional coherency strains between two individual monolayers. These coherency strains, or patterns that arise due to misaligned atoms in monolayers, are induced by differing bond lengths of the separate layers. They can arise as a result of different materials and/or geometries. We will introduce a phenomenological model that will be used to analyze the effects of stretching, bending, and van der Waals (vdW) interactions on the resulting structures.

Once these equilibrium structures have been examined, we will explore the effects of finite temperatures on those structures, where these thermal effects will be incorporated by means of a Langevin model. Each monolayer will be approximated as a chain of atoms under the influence of periodic boundary conditions. In particular, there will be two separate monolayers in our model; the bottom chain will act as the

inner/substrate layer and will be assumed to be rigid, while the top chain will act as the outer layer and will be allowed to move freely according to the forces described above.

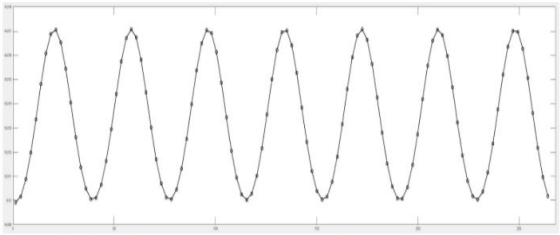

A chain that represents the outermost layer of the multi-wall carbon nanotube to the right

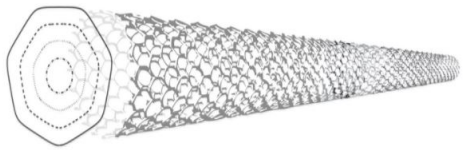

A cross section schematic of a multi-walled carbon nanotube exhibiting polygonization.

Figure 1.1: Typical cross section of a multi-walled carbon nanotube.

Multiwalled nanotubes have the structure of nested cylinders formed by monolayers, or singular sheets of atoms, rolled up to create the walls of the nanotube.[16] A consequence of this geometry is that more atoms are needed in the outer walls of the nanotube as opposed to the inner walls. These extra atoms can cause unidirectional coherency strains between the two neighboring walls. The strains can affect the physical properties of the nanotube.

We construct a model that describes two different monolayers. We will fix the lower monolayer, or what we call the substrate. The top monolayer will be allowed to move freely, dictated by the forces acting on it. Doing this allows us to see the effects of extra atoms in the upper monolayer.

We will be incorporating three separate forces on the atoms in the free monolayer. These will be the van der Waals between the two monolayers, a bonding energy between neighboring atoms in the free monolayer to keep it together, and a bending energy that imposes a resistance to bending. Along with these different forces, we will impose periodic boundary conditions. The substrate will have its atoms a fixed uniform distance apart. We will then give the free monolayer different initial positions and the forces varying strengths to analyze the effects of extra atoms in the free monolayer and where they come to equilibrium.

Our model predicts the equilibrium configurations of the monolayer. We then apply a thermostat to the model so see the effects of temperature on these equilibrium structures. As the original model only includes the forces, there is no temperature, which is naturally unrealistic. To incorporate thermal effects into our system, we will need a stochastic (Langevin) model. We will slowly increase the temperature to our desired temperature to ensure that the effects that occur are solely from the current temperature and not the increase in temperature.

To study the effects of the strengths of the energies acting on the free monolayer, we will only be varying three constants during our experiment. The constants represent the strength of each energy. To properly study the effects of the relative strength of each energy, we will fix the number of atoms in both layers, the free layer will contain one more atom. This could correspond to a system such as a two-walled nanotube in which the outer wall has one additional atom in it. We will normalize the spacing between atoms in the substrate and the vdW radius and we will use a

uniform layer as the initial condition. We vary our three parameters to create several combinations of energy strengths. We expect to see different shapes and magnitudes of said shapes.

The first thing we notice is that, since there is one more atom in the free layer compared to the substrate, there is a single peak that forms. This peak varies in shape and size based on our three parameters. When the van der Waals strength is increased, we see that the peak tends to decrease in size. When the strength of the bonding energy is increased, the amplitude slightly increases and broadens the overall shape. Increasing the strength of the bending energy, we see that the peak goes from a sharp point to a more smoothly rounded shape.

After exploring these different combinations, we examine a more realistic model. We apply parameters that are seen in graphene. After applying these parameters, the results show us that we see a more rounded shape that is moderately sized. Applying the parameters of graphene, we gain some insight into the response of bilayer graphene.

Now that we have acquired different equilibrium structures of our free monolayer, we wish to see how temperature affects these structures. We use our stochastic model to incorporate temperature. We slowly increase the temperature until we reach our desired temperature. We increase the temperature slowly as to avoid the change in temperature being the cause of change in our structures. After applying different maximum temperatures, we see that the structures begin to stray away from the standard one peak structure and start to form many smaller peaks. When the tem-

perature reaches a threshold, we see that the single peak disappears and is replaced with many different peaks of various sizes.[24]

Another model we derive is that in which indentations are incorporated. We explore what occurs when the substrate contains a hole, or has some atoms removed from it. With this hole in the substrate, we add a constant force that acts upon a specified number of atoms in the top layer that pushes downward, perpendicular to the substrate. An increase in strength of the constant is shown to increase the deflection, or total displacement from the initial position, of the top layer.

It also is discovered that the length of the bonds in the top layer increases the deflection of the top layer. If the distance between atoms in the substrate decreases, it makes the it more difficult for the top layer to potentially cross through the hole in the substrate. When the length of the vdW radius is increased, the top layer is pushed farther away from the substrate, increasing the top layer's height. We also investigate conditions under which the top layer fully crosses through the hole in the substrate. Through numerical simulations we discover that there does exist a set of parameters in which this crossing occurs.

CHAPTER II

BACKGROUND

We now discuss some of the background knowledge that is needed to understand the phenomena that we model.

2.1 Brownian Motion

In 1827, botanist Robert Brown observed the sporadic motion of particles. Brown observed the grains of pollen of the clarkia pulchella plant in water under a microscope and saw that the particles were in a continuous and unpredictable motion. He then examined that this motion occurred with other materials in water, such as fossilized wood and glass, and again saw this behavior under the microscope. He used these materials to explore if the observed motion had something to do with life within the material, as the plant particles were alive. Brown attempted to form various explanations for why these particles were behaving in this manner, but was unable to do so. Brown was credited for the discovery of this behavior and we now refer to this type of motion as Brownian Motion.

Many years later, the kinetic theory of heat was developed by multiple scientists, most notably Maxwell and Boltzmann. They concluded that the Brownian motion of the particles was caused by fluid molecules bouncing off the particles. It

was then reasoned that the particles were gaining kinetic energy in the form of heat energy. In 1988, Léon Gouy looked further into this and noticed that the random motion was generated due to thermal molecular collisions.[25]

2.1.1 Theory of Diffusion

In 1905, Albert Einstein began to investigate mathematical models that described the diffusion of atoms suspended in a liquid. He developed a relation between the diffusion constant and the mean square displacement,

$$\langle (x(t) - x_0)^2 \rangle = 2Dt, \tag{2.1}$$

where $x(t)$ is the position of a particle at time t, x_0 is the initial position of the particle, $\langle \cdot \rangle$ is the average, and D is the coefficient of diffusion.

Next, we derive an expression for the diffusion coefficient D. Assume first that there are randomly distributed particles suspended in a liquid. Now assume that a force K, which is solely dependent on position, acts on those particles. Next assume that the number of suspended particles per unit volume is ν, which is a function of position, x, in the case of thermodynamic equilibrium. We will denote the arbitrary virtual displacement as δx. We let A denote the free energy of the system, U the internal energy, T the absolute temperature, and S the entropy. We know that the free energy must vanish, therefore, using the definition of Helmholtz free energy,

$$A = U - TS. \tag{2.2}$$

Therefore, the change in the energy, δA, is

$$\delta A = \delta U - T\delta S \tag{2.3}$$

where δU is the change in internal energy and δS denotes the change in entropy.[26] Since we desire thermal equilibrium, we get that

$$\delta A = \delta U - T\delta S = 0. \tag{2.4}$$

Next, we will assume that the liquid has a unit cross section orthogonal to the x-axis with bounding planes $x = 0$ and $x = l$. We then have the following equation for the total internal energy,

$$\delta U = -\int_0^l K\nu\delta x dx, \tag{2.5}$$

and the following equation for the entropy,

$$\delta S = \int_0^l R\frac{\nu}{N}\frac{\partial\delta x}{\partial x}dx = -\frac{R}{N}\int_0^l \frac{\partial\nu}{\partial x}\delta x dx. \tag{2.6}$$

We assume that the liquid the particles are suspended in has a unit cross section perpendicular to the x-axis and is bounded by two planes, we can integrate equations (2.5) and (2.6) and substitute the results into equation (2.4) to derive the required equilibrium condition to be

$$-K\nu + \frac{RT}{N}\frac{\partial\nu}{\partial x} = 0. \tag{2.7}$$

It follows that the right term is equal to the partial of the pressure, p with respect to x or

$$-K\nu + \frac{\partial p}{\partial x} = 0. \tag{2.8}$$

Equation (2.8) implies that the force K must be equilibrated by the force of osmotic pressure. If we assume that the particles are spherical, with radius a, and the viscosity of the liquid has coefficient μ, we know that the force K gives the particles the velocity[27]

$$\frac{K}{6\pi\mu a}. \tag{2.9}$$

Since ν represents the particles per unit volume, multiplying ν by the velocity of an atom gives us the number of particles passing through a unit area per unit time, which is

$$\frac{\nu K}{6\pi\mu a}. \tag{2.10}$$

If we denote the diffusion coefficient of the suspended particles as D, we get that

$$-D\frac{\partial \nu}{\partial x} \tag{2.11}$$

particles will pass through a unit area per unit time due to diffusion. This is the case as $\frac{\partial \nu}{\partial x}$ represents the change in the total number of particles at position x and D represents the diffusion, which describes how the particles spread through an area. Because of dynamic equilibrium

$$\frac{\nu K}{6\pi\mu a} - D\frac{\partial \nu}{\partial x} = 0. \tag{2.12}$$

Combining conditions (2.7) and (2.12), we get

$$D = \frac{RT}{N}\frac{1}{6\pi\mu a}. \tag{2.13}$$

as the diffusion coefficient.[28]

2.2 Modeling Thermal Effects

Consider the motion of a particle moving along a straight line. Let $x(t)$ denote the position of the particle at time t. Our standard equation of motion for the particle, derived from Newtons second law, is

$$m\frac{d^2x}{dt^2} = F - \gamma\frac{dx}{dt}, \tag{2.14}$$

where F is the sum of forces acting on the particle and the second term on the right-hand side is friction. The issue that we run into is that this equation does not account for any thermal effects. Next we discuss an approach for including thermal effects in (2.14).

We are interested in thermal effects in an equation like (2.14) because later we will simulate structures composed of particles. The thermal effects we consider allow us to explore the way temperature affects different structures and how it higher temperature can destabilize the equilibrium shapes of those structures. To model the thermal effects for our system, we will be using the Langevin equation. The Langevin equation is a second order (first order with respect to velocity) stochastic differential equation. It is known as one of the simplest for creating a mathematical model of Brownian motion. What makes this equation stochastic is the fact that there is a random force term.[29] This random force term is where the thermal effects are described. We will elaborate on how this term models thermal effects shortly.

2.2.1 Langevin Equation

As shown previously, we know that the coefficient of diffusion is described in equation (2.13). Einstein was the first to prove this. Paul Langevin then attempted to prove this to be true using a different approach. He created an equation that we now refer to as the Langevin equation. The equation is

$$m\frac{d^2x}{dt^2} = F - \gamma\frac{dx}{dt} + X(t) \tag{2.15}$$

Here $X(t)$ represents the random forces whose average is zero. By assuming that the particles are spherical, we can assume Stokes' law. This implies that the particles experience a resistance of $\gamma = 6\pi\mu a$, where μ is the viscosity of the liquid and a is the radius of the particles.[30] Langevin derived that the general solution to equation (2.15) is

$$\langle (x(t) - x_0)^2 \rangle = \frac{RT}{N}\frac{1}{3\pi\mu a}t. \tag{2.16}$$

This allows us to extract the diffusion coefficient as

$$D = \frac{RT}{N}\frac{1}{6\pi\mu a}. \tag{2.17}$$

by equation (2.1). This shows that the same result Einstein derived can be established from the Langevin equation.[31]

2.2.2 Fluctuation-Dissipation Theorem

Returning to Langevin's equation, equation (2.15), we will now begin to find the solution and see how this compares to the expected mean square velocity, which describes the velocity particles at thermal equilibrium. At thermal equilibrium,

$\langle v(t)^2 \rangle = k_B T/m$, where k_B is the Boltzmann constant and T is the temperature. The force $X(t)$ in (2.15) is random but satisfies statistical requirements. These requirements include that X must follow the Maxwell-Boltzmann distribution. Also, letting t and t' be different instances of time that have no correlation, the force, X, has the following averages over an infinitesimal time interval,

$$\langle X(t) \rangle = 0,$$

$$\langle X(t)X(t') \rangle = 2B\delta(t - t'). \tag{2.18}$$

Since we are requiring the noise term to be defined by the means of a delta function, we can refer to this noise as a white noise term. The constant B in (2.18) denotes the strength of the fluctuating force. Solving the Langevin equation for the velocity, or first derivative of the position, we get

$$\frac{dx}{dt} = v(t) = v(0)e^{-\frac{\gamma t}{m}} + \int_0^t \frac{e^{-\frac{\gamma(t-t')}{m}} X(t')}{m} dt'. \tag{2.19}$$

From here we want to develop an expression for the expected mean square velocity. So we must first find $v^2(t)$. We have

$$v(t)^2 = \left(v(0)e^{-\frac{\gamma t}{m}} + \int_0^t \frac{e^{-\frac{\gamma(t-t')}{m}} X(t')}{m} dt' \right)^2$$

$$= \left(v(0)e^{-\frac{\gamma t}{m}} \right)^2 + 2v(0)e^{-\frac{\gamma t}{m}} \int_0^t \frac{e^{-\frac{\gamma(t-t')}{m}} X(t')}{m} dt' + \left(\int_0^t \frac{e^{-\frac{\gamma(t-t')}{m}} X(t')}{m} dt' \right)^2 \tag{2.20}$$

Over time, we see that the first term decays to zero and thus does not add to the mean square velocity at thermal equilibrium. Averaging the cross term, we see that it decays to zero as well due to the exponential. Looking now to the third term,

we see that is a second-order noise term, or a noise term to the second power. Using the conditions in (2.18), taking the average of this term and integrating twice, we get

$$\langle v(t)^2 \rangle = v(0)^2 e^{-\frac{2\gamma t}{m}} + \frac{B}{\gamma m}\left(1 - e^{-\frac{2\gamma t}{m}}\right). \tag{2.21}$$

As time goes to infinity, we see that the exponentials will decay to zero, leaving us with

$$\langle v(t)^2 \rangle = \frac{B}{\gamma m}. \tag{2.22}$$

We expect that this should be the same as the expected mean square velocity at thermal equilibrium, thus

$$\langle v(t)^2 \rangle = \frac{B}{\gamma m} = \frac{k_B T}{m}, \tag{2.23}$$

which then gives us the relation

$$B = \gamma k_B T. \tag{2.24}$$

This is the fluctuation-dissipation theorem. Essentially, the strength of the fluctuation, B, and the magnitude of the friction or dissipation, γ, are related. This allows the system to be balanced between fluctuation and dissipation so that thermal equilibrium may be achieved.[32]

2.3 Equation of Motion for Particles at Thermal Equilibrium

The derivation of the equation of motion begins with the Langevin equation. As we will need to incorporate external forces, those that do not relate to thermal forces, we will add a term, F, to represent the sum of all external forces. Recall from

above that this gives

$$m\frac{d^2x}{dt^2} = F - \gamma\frac{dx}{dt} + X(t). \tag{2.25}$$

As seen in the previous section, we know that the relation between the fluctuation and dissipation is given by $B = \gamma k_B T$. Going back to the conditions on $X(t)$ that were described in eq. (2.18), we can replace B to get

$$\langle X(t)\rangle = 0,$$

$$\langle X(t)X(t')\rangle = 2\gamma k_B T\delta(t-t') \tag{2.26}$$

If we let $X(t) = A\eta(t)$ and give $\eta(t)$ the conditions

$$\langle \eta(t)\rangle = 0,$$

$$\langle \eta(t)\eta(t')\rangle = \delta(t-t'), \tag{2.27}$$

we can use equation (2.26) to solve for A. This yields

$$\langle X(t)X(t')\rangle = \langle A\eta(t)A\eta(t')\rangle,$$

$$2\gamma k_B T\delta(t-t') = A^2\delta(t-t'),$$

$$A = \sqrt{2\gamma k_B T}. \tag{2.28}$$

Thus $X(t) = \sqrt{2\gamma k_B T}\eta(t)$, which results in the equation

$$m\frac{d^2x}{dt^2} = F - \gamma\frac{dx}{dt} + \sqrt{2\gamma k_B T}\eta(t) \tag{2.29}$$

CHAPTER III

MODEL OF ATOMIC CHAIN INTERACTING WITH A SUBSTRATE

In this chapter we develop the model we use to predict the equilibrium configurations of an atomic chain with a rigid substrate.

3.1 External Forces

The equation of motion used for each individual atom was shown in equation (2.14). We will adjust this equation to fit the vector notation we will be using, which gives us

$$m\frac{d^2\mathbf{r}_i}{dt^2} = \mathbf{F}_i - \gamma\frac{d\mathbf{r}_i}{dt}, \tag{3.1}$$

where $\mathbf{r}_i$ is the vector representing the location of atom i in the monolayer. The term $\mathbf{F}_i$ represents the sum of the total external forces acting on atom i.

The equation of motion used for each individual atom with temperature included written in vector notation is

$$m\frac{d^2\mathbf{r}_i}{dt^2} = \mathbf{F}_i - \gamma\frac{d\mathbf{r}_i}{dt} + \sqrt{2\gamma k_B T}\boldsymbol{\eta}_i \tag{3.2}$$

where k_B is the Boltzmann constant, T is the temperature, and $\boldsymbol{\eta}_i$ is a standard white noise term satisfying the fluctuation-dissipation theorem, all discussed in the previous chapter.

The external forces are related to the potential energy of the forces acting on the atoms of the monolayer. The part of the total potential energy that depends on the position of atom i, U_i, will be a sum of three different potential energies; the first is the van der Waals (vdW) interaction between atom i in the monolayer and the substrate, $U_{i,1}$, the second one measures the elastic stretching energy that holds between atom i and its nearest neighbor on each side in the monolayer together, $U_{i,2}$, and the last one measures the elastic bending energy between atom i and its two nearest neighbors on each side in the monolayer, $U_{i,3}$.

The equation that describes the potential energy, U_i, is,

$$U_i = U_{i,1} + U_{i,2} + U_{i,3}. \tag{3.3}$$

We now can use this to develop our equation for the external forces. The external forces on atom i will be the negative gradient of the potential energy with respect to the position of atom i. Thus, our equation for the external forces is as follows,

$$\mathbf{F}_i = -\nabla_{\boldsymbol{r}_i} U_i = -\nabla_{\boldsymbol{r}_i} U_{i,1} - \nabla_{\boldsymbol{r}_i} U_{i,2} - \nabla_{\boldsymbol{r}_i} U_{i,3}. \tag{3.4}$$

For notation purposes, we will denote the total number of atoms in the top chain by N and in the bottom chain by M. The difference vectors between neighboring atoms, $\mathbf{b}_i$, and will be defined as $\mathbf{b}_i = \mathbf{r}_{i+1} - \mathbf{r}_i$.

3.1.1 Van der Waals Energy

The weak attraction between the separate monolayers is dominated by the so-called van der Waals (vdW) interaction. To model this force, we start with the

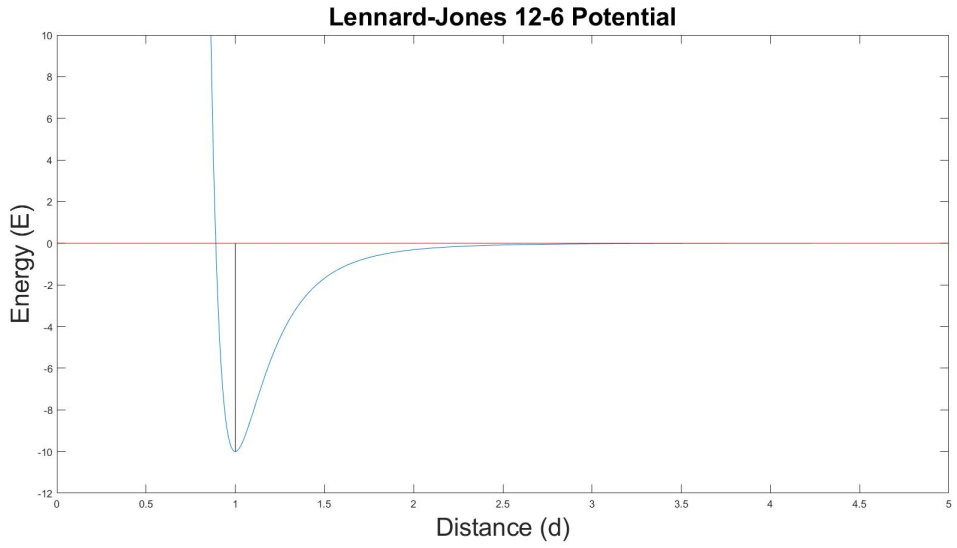

Figure 3.1: Profile of the Lennard-Jones (12-6) potential as a function of inter-particle spacing in units of the vdW radius σ.

well-studied Lennard-Jones (or "12-6") potential between two atoms given by

$$U_{\mathrm{LJ}} = \epsilon \left[\left(\frac{\sigma}{d} \right)^{12} - 2 \left(\frac{\sigma}{d} \right)^{6} \right], \tag{3.5}$$

where ϵ as the depth of the potential well, σ as the vdW radius, and d as the distance between the two atoms. In Figure 1, we show a typical profile of the vdW interaction as a function of distance in units of σ. It can be seen that the energy is zero if the distance between the atoms is to σ. We also notice that the black line shows the depth of the well ϵ, where here $\epsilon = 10$. Finally, we see that the energy asymptotically vanishes as the spacing becomes infinitely far apart.

Using equation (3.5) and $\mathbf{d}_{i,j}$ as the vector describing the distance between atom i in the monolayer and atom j in the substrate, we will find the total vdW

energy as a sum of the energetic contributions from each atom in the top chain as

$$U_{i,1} = \epsilon \sum_{j=1}^{M} \left[\left(\frac{\sigma}{\|\mathbf{d}_{i,j}\|} \right)^{12} - 2 \left(\frac{\sigma}{\|\mathbf{d}_{i,j}\|} \right)^{6} \right] \tag{3.6}$$

Taking the negative gradient of Equation (3.6), we obtain the force

$$-\nabla_{\boldsymbol{r}_i} U_{i,1} = \frac{12\epsilon}{\sigma} \sum_{j=1}^{M} \left[\left(\frac{\sigma}{\|\mathbf{d}_{i,j}\|} \right)^{13} - \left(\frac{\sigma}{\|\mathbf{d}_{i,j}\|} \right)^{7} \right] \frac{\mathbf{d}_{i,j}}{\|\mathbf{d}_{i,j}\|} \tag{3.7}$$

3.1.2 Elastic Energy

To keep the atoms in the top chain connected to one another, we will use an elastic energy that will act as a linear spring. We will use k_s as the bond strength and l as the natural length of the bonds. This will give us the potential energy of the elastic interactions as

$$U_{i,2} = \frac{k_s}{2} \left[(\|\mathbf{b}_{i-1}\| - l)^2 - (\|\mathbf{b}_i\| - l)^2 \right]. \tag{3.8}$$

Taking the negative gradient of equation 3.8, we obtain the elastic force

$$-\nabla_{\boldsymbol{r}_i} U_{i,2} = -k_s \left[(\|\mathbf{b}_{i-1}\| - l) \frac{\mathbf{b}_{i-1}}{\|\mathbf{b}_{i-1}\|} - (\|\mathbf{b}_i\| - l) \frac{\mathbf{b}_i}{\|\mathbf{b}_i\|} \right]. \tag{3.9}$$

3.1.3 Bending Energy

Finally, to prevent the chain of atoms from collapsing in on itself, we will add in an energy that acts as a resistance to bending in the form of a torsional spring. To do this, we first need to calculate the angles, θ_i, that the vectors $\mathbf{b}_i$ makes with the positive x-axis. The angles, θ_i, are allowed to range from $(-\infty, \infty)$. To prevent the bending of the atoms, we want the difference between neighboring atom bond angles to be minimized. This implies that the bonds have the same angle and that

the chain is straight. Using k_b as the strength of the bending resistance, we get a potential energy as

$$U_{i,3} = \frac{k_b}{2} \sum_{k=i-2}^{i} (\theta_{k+1} - \theta_k)^2 . \tag{3.10}$$

Expanding out the summation yields

$$U_{i,3} = \frac{k_b}{2} \left[(\theta_{i-1} - \theta_{i-2})^2 + (\theta_i - \theta_{i-1})^2 + (\theta_{i+1} - \theta_i)^2 \right] .$$

Here we have that

$$\theta_i = \arctan \left(\frac{\mathbf{b}_{i,y}}{\mathbf{b}_{i,x}} \right) .$$

The following gradients are needed

$$\nabla_{\boldsymbol{r}_i} \theta_i = -\frac{1}{\|\mathbf{b}_i\|^2} \begin{pmatrix} \mathbf{b}_{i,y} \\ -\mathbf{b}_{i,x} \end{pmatrix}$$

$$\nabla_{\boldsymbol{r}_i} \theta_{i-1} = -\frac{1}{\|\mathbf{b}_{i-1}\|^2} \begin{pmatrix} -\mathbf{b}_{i-1,y} \\ \mathbf{b}_{i-1,x} \end{pmatrix} .$$

Taking the negative gradient, with respect to atom i, of Equation (3.10) expanded out,

$$\begin{aligned} -\nabla_{\boldsymbol{r}_i} U_{i,3} = k_b \, [& -(\theta_{i-1} - \theta_{i-2}) \cdot \nabla_{\boldsymbol{r}_i} \theta_{i-1} - (\theta_i - \theta_{i-1}) \cdot \nabla_{\boldsymbol{r}_i} \theta_i \\ & + (\theta_i - \theta_{i-1}) \cdot \nabla_{\boldsymbol{r}_i} \theta_{i-1} + (\theta_{i+1} - \theta_i) \cdot \nabla_{\boldsymbol{r}_i} \theta_i] . \end{aligned}$$

Using the gradients for θ_i and θ_{i-1} found above,

$$-\nabla_{\boldsymbol{r}_i} U_{i,3} = k_b \left[\frac{\theta_i - \theta_{i-1}}{\|\mathbf{b}_{i-1}\|^2} \begin{pmatrix} -\mathbf{b}_{i-1,y} \\ \mathbf{b}_{i-1,x} \end{pmatrix} + \frac{\theta_{i+1} - \theta_i}{\|\mathbf{b}_i\|^2} \begin{pmatrix} \mathbf{b}_{i,y} \\ -\mathbf{b}_{i,x} \end{pmatrix} \right.$$
$$\left. + \frac{\theta_{i-2} - \theta_{i-1}}{\|\mathbf{b}_{i-1}\|^2} \begin{pmatrix} -\mathbf{b}_{i-1,y} \\ \mathbf{b}_{i-1,x} \end{pmatrix} + \frac{\theta_{i-1} - \theta_i}{\|\mathbf{b}_i\|^2} \begin{pmatrix} \mathbf{b}_{i,y} \\ -\mathbf{b}_{i,x} \end{pmatrix} \right].$$

By combining like terms, we obtain the bending force

$$-\nabla_{\boldsymbol{r}_i} U_{i,3} = k_b \left[\mathbf{A}_i + \mathbf{B}_i \right] \tag{3.11}$$

where

$$\mathbf{A}_i = \frac{\theta_{i+1} - 2\theta_i + \theta_{i-1}}{\|\mathbf{b}_i\|^2} \begin{pmatrix} \mathbf{b}_{i,y} \\ -\mathbf{b}_{i,x} \end{pmatrix},$$

$$\mathbf{B}_i = \frac{\theta_i - 2\theta_{i-1} + \theta_{i-2}}{\|\mathbf{b}_{i-1}\|^2} \begin{pmatrix} -\mathbf{b}_{i-1,y} \\ \mathbf{b}_{i-1,x} \end{pmatrix}.$$

We now have the forces associated with all three potential energies and are able to study equilibrium structures that result from different strengths of the three energies. Before we study equilibrium structures, we first discuss the numerical methods used to solve the model.

3.2 Numerical Methods

There are two different approaches that will be taken to simulate the response of chains of atoms. Both approaches start from the equations of motion given by applying Newton's Second Law. The first of these is to find equilibrium solutions

using the gradient flow model. For this approach the temperature is fixed at zero. The second approach uses the Velocity Verlet integrator to solve the Langevin equations. We also find a distance bound for the vdW energy as we cannot numerically calculate a force over an infinite distance.

3.2.1 Gradient Flow

Our equation of motion without temperature, equation (2.29) where $T = 0$, is a second order differential equation. When the time comes for us to numerically solve this using a standard ordinary differential equation solver, we have to construct a system of first order differential equations. Since the equation is of second order, we must create two first order equations for our direction along one direction. If we wish to let our model be two dimensional, we will have to create two first order equations for each dimension, implying four equations for each atom. If we plan to create our model with one hundred atoms, this implies that we will need to solve four hundred equations for at each time step. Although many programs can handle these many equations, the program will be slow. There is a way to cut the number of equations in half.

Since we are modeling atoms, we know that the mass is very small. If we then assume the mass to be zero, the equation of motion, equation (2.29) with $T = 0$, simplifies to

$$0 = F - \gamma \frac{dx}{dt}, \tag{3.12}$$

which then gives us the first order differential equation

$$\frac{dx}{dt} = \frac{1}{\gamma}F. \tag{3.13}$$

We know that the equation of motion for each atom is expressed in equation (3.1). Using that the force term, $\boldsymbol{F}_i$, is equal to the negative gradient of the potential energy, $-\nabla_{\boldsymbol{r}_i} U_i$, we can rewrite the equation as

$$m\frac{d^2\mathbf{r}_i}{dt^2} = -\nabla_{\boldsymbol{r}_i} U_i - \gamma\frac{d\mathbf{r}_i}{dt}, \tag{3.14}$$

where $-\nabla_{\boldsymbol{r}_i} U_i$ is described in equation (3.4).

We also noted that a system of first order differential equations allows us to solve for the equilibrium configurations of the chain efficiently, the gradient flow model. If we take that equation, equation (3.13), and rewrite it in vector form and with the negative potential energy as our force term, we get

$$\frac{d\boldsymbol{r}_i}{dt} = -\frac{1}{\gamma}\nabla_{\boldsymbol{r}_i} U_i. \tag{3.15}$$

This equation benefits us as it has now been reduced to a first order equation, meaning for each dimension of an atom there is only one needed equation instead of two. This cuts the number of equations that need to be solved in half as desired. This model allows us to solve for equilibrium states faster when no temperature is included. This model will not be useful once temperature is included. For this reason, we also use the velocity Verlet algorithm.

3.2.2 Velocity Verlet

In his physical review, Loup Verlet used a simple algorithm to numerically integrate for the position of particles described by Newton's Second Law of Motion

$$m\frac{d^2\mathbf{r}}{dt^2}(t) = m\mathbf{a}(t) = \mathbf{F}(t). \tag{3.16}$$

The algorithm uses the Taylor series expansions of order three of $\mathbf{r}_i(t+h)$ and $\mathbf{r}_i(t-h)$, where h is the time increment and $\mathbf{r}_i(t)$ is the position of particle i at time t. The expansions are

$$\begin{aligned}\mathbf{r}_i(t+h) &= \mathbf{r}_i(t) + \mathbf{v}_i(t)h + \frac{1}{2}\mathbf{a}_i(t)h^2 + \frac{1}{6}\mathbf{d}_i(t)h^3 \\ \mathbf{r}_i(t-h) &= \mathbf{r}_i(t) - \mathbf{v}_i(t)h + \frac{1}{2}\mathbf{a}_i(t)h^2 - \frac{1}{6}\mathbf{d}_i(t)h^3\end{aligned} \tag{3.17}$$

where $\mathbf{v}_i(t)$ is the velocity of particle i at time t, $\mathbf{a}_i(t)$ is the acceleration of particle i at time t, and $\mathbf{d}_i(t)$ is the third deriative of $\mathbf{r}_i$ at time t. Summing these expansions gives us[33]

$$\mathbf{r}_i(t+h) = -\mathbf{r}_i(t-h) + 2\mathbf{r}_i(t) + \mathbf{a}_i(t)h^2, \tag{3.18}$$

Using equation (3.18) to approximate solutions to equation (3.16) is known as the Verlet algorithm. Since we desire to keep track of the velocities of each atom, we want to use a slight variation of this algorithm. We begin by using the following equation for velocity

$$\mathbf{v}_i(t) = \frac{\mathbf{r}_i(t) - \mathbf{r}_i(t-h)}{h} \tag{3.19}$$

to rewrite equation (3.18) as

$$\mathbf{r}_i(t+h) = \mathbf{r}_i(t) + \mathbf{v}_i(t)h + \mathbf{a}_i(t)h^2. \tag{3.20}$$

We can also calculate the total velocity of a particle using the sum of the acceleration at the current and next time steps, t and $t+h$ respectively, to get

$$\mathbf{v}_i(t+h) = \mathbf{v}_i(t) + \frac{1}{2}\left(\mathbf{a}_i(t) + \mathbf{a}_i(t+h)\right)h. \tag{3.21}$$

Using equation (3.16), we can rewrite equations (3.20) and (3.21) to get

$$\mathbf{r}_i(t+h) = \mathbf{r}_i(t) + \mathbf{v}_i(t)h + \frac{1}{m_i}\mathbf{f}(\mathbf{r}_i(t))h^2$$

$$\mathbf{v}_i(t+h) = \mathbf{v}_i(t) + \frac{1}{2m_i}[\mathbf{f}(\mathbf{r}_i(t)) + \mathbf{f}(\mathbf{r}_i(t+h))]h. \tag{3.22}$$

Using these formulas to approximate solutions to equation (3.16) is known as the velocity Verlet algorithm. The purpose of this algorithm is that it allows us to integrate for the position of all atoms, while minimizing the roundoff error, as this algorithm has error of fourth order, $O(h^4)$, as the Taylor series expansion of order three was used, while giving a stable numerical solution.[34]

3.2.3 Bound for vdW Energy

For numerical purposes, this interaction must be truncated at some finite distance. To figure out what distance is needed to get an approximation that satisfies a certain tolerance, we will bound the error in the energy with the value $-\xi$, where the minus sign is taken as the energy will be negative when the distance is larger than σ. We must therefore solve for

$$-\xi \geq \epsilon\left[\left(\frac{\sigma}{d}\right)^{12} - 2\left(\frac{\sigma}{d}\right)^{6}\right]. \tag{3.23}$$

Substituting $x = \left(\frac{\sigma}{d}\right)^6$, we obtain

$$0 \geq x^2 - 2x + \frac{\xi}{\epsilon},.$$

Setting the right hand side equal to zero, we get the following solutions for x

$$x = 1 \pm \sqrt{1 - \frac{\xi}{\epsilon}}.$$

Taking the positive root, which is the physically relevant root, and returning to the original parameters yields the cutoff radius

$$d \geq \frac{\sigma}{\sqrt[6]{1 - \sqrt{1 - \frac{\xi}{\epsilon}}}}. \tag{3.24}$$

For example, a tolerance of $\xi = \epsilon/1000$ gives a radius of $d \geq 3.55\sigma$, which corresponds to an energy accurate to one thousandth of the well depth. We thus only need to include atoms within that radius for the vdW calculation to achieve a solution that maintains this desired level of accuracy.

CHAPTER IV

EQUILIBRIUM STRUCTURES

In this chapter we explore various equilibrium structures that arise as we vary the relative strengths of the different forces in our model. Since we are examining the relationship between the forces based on the potential energies described in the previous chapter, temperature will not be included.

4.1 Solving for Equilibrium Structures

For our simulations, we use the cross-section of two monolayers. The bottom layer, or what we call the substrate, will be fixed. The top layer will be allowed to move around freely in the plane, according to the forces acting on it. In figure 4.1 we see an example of what the initial configuration may look like.

We begin each numerical simulation with each atom in the free layer at a uniform height from the substrate and a uniform distance apart. We then use the system of equations (3.15) for $i = 1, \ldots, N$ to solve for the equilibrium state of the free layer. Recall that N is the number of atoms on the cross-section of the free layer. For each experiment, we will vary the strength of each one of our potential energies that were described above. We analyze each equilibrium structure to see the effects each energy has on the free layer. We will also explore the equilibrium structure

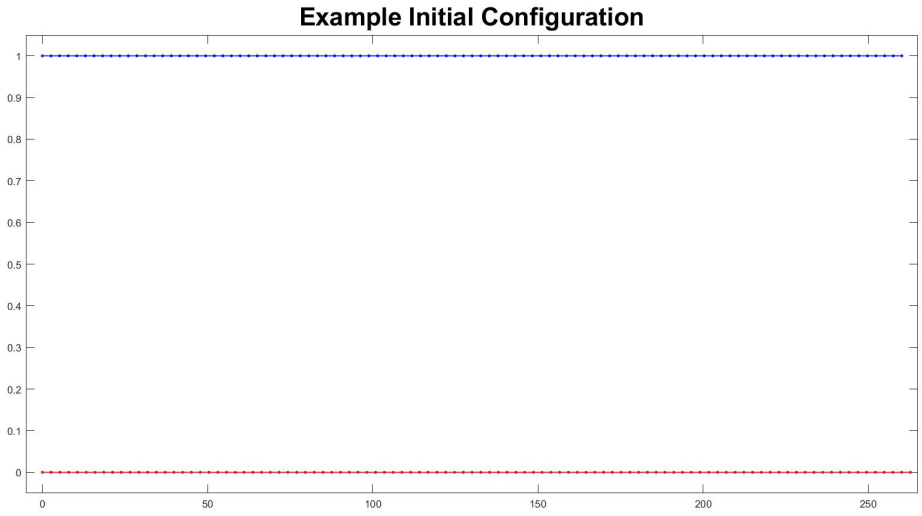

Figure 4.1: An example of an initial configuration.

of the free layer if we set all parameters to values consistent with the properties of graphene.

To numerically solve for equilibrium structures, we use Matlab's built-in ordinary differential equation solver, ode45. Matlab's solver is efficient as it is optimized. Numerically solving the gradient flow equations should yield solutions that approach equilibrium configurations minimizing the total energy. To determine when equilibrium has been attained, we set a numerical tolerance. After a set number of time steps, the overall absolute value of the displacement of each atom, from its previously checked position, will be summed and if the total is smaller than the tolerance, the system will be deemed to be equilibrated. The simulation is then ended, and the final position of the atoms will define the equilibrium structure of the free layer.

For atoms on the free layer, we assume periodic boundary conditions. To

implement these conditions, ghost atoms are used. We place two ghost atoms at the left end and two ghost atoms at the right end of the free layer. The y-positions are dictated by the y-position from the first two real atoms on the opposite side. The x-position is dictated by taking the x-position from the two real atoms on the opposite side and by adding or subtracting the length of the system, which is the original length of the free layer plus the original distance between two atoms. This allows for all the forces to be calculated in a way that mimics the ends of the chain as being connected. The ghost atoms are included in the computation of the stretching and bending forces that act on the two atoms at the left end and the two atoms at the right end of the free layer at each time step.

4.2 Paramteric Study of Equilibrium Configurations

Without loss of generality, we will only be varying three constants during our experiment. These three constants are the moduli of the forces corresponding to the three energies. The constants will be denoted as follows: ϵ for the vdW interactions, k_s for the bonds, and k_b for the bending.

We will normalize the spacing between atoms in the substrate to 1, the vdW radius to $\sigma = 1$. To properly study the effects of each strength, we will fix the number of atoms in both chains, the free chain will contain one more atom, N, than the substrate, M ($N = 101$, $M = 100$). An example of this initial configuration is shown in figure 4.1. The free chain atoms will all be contained horizontally between the two end atoms on the substrate.

We will use the set {0.1, 1, 10} as the range of values in which we will vary the strengths of each force. We will explore all the combinations of values to see how each force affects the overall shape of the structure and how the magnitudes of each strength interact with each other. In the figures below, we show a subset of the equilibrated configurations predicted by the simulations.

In some of the figures, there are green and red numbers. These numbers represent the amplification of the peaks, of the same color. This allows us to gain a better view of the shapes of the peaks.

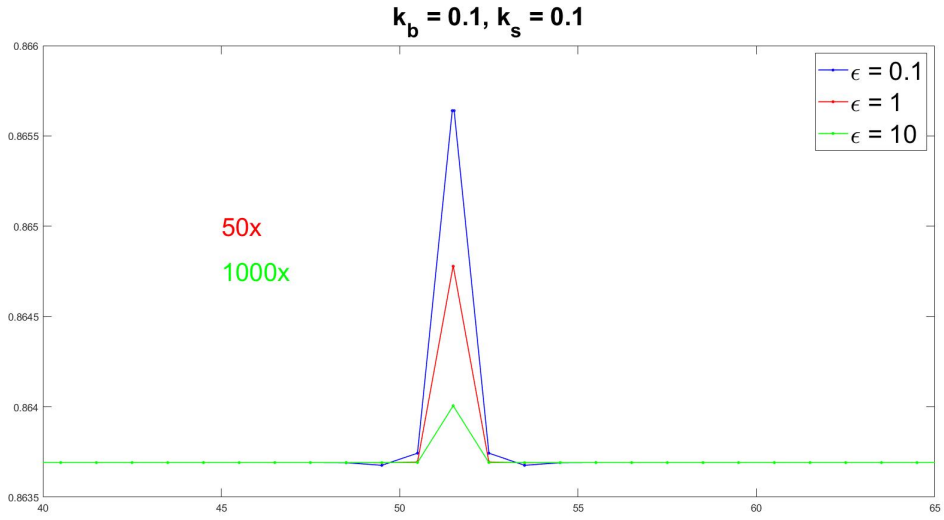

Figure 4.2: Here the red peak is amplified by a factor of 50, the green by 1000.

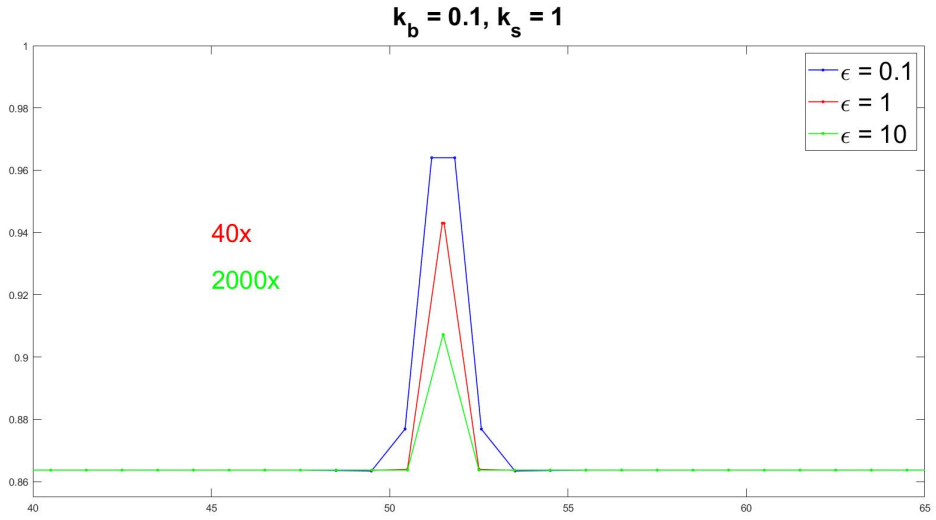

Figure 4.3: Here the red peak is amplified by a factor of 40, the green by 2000.

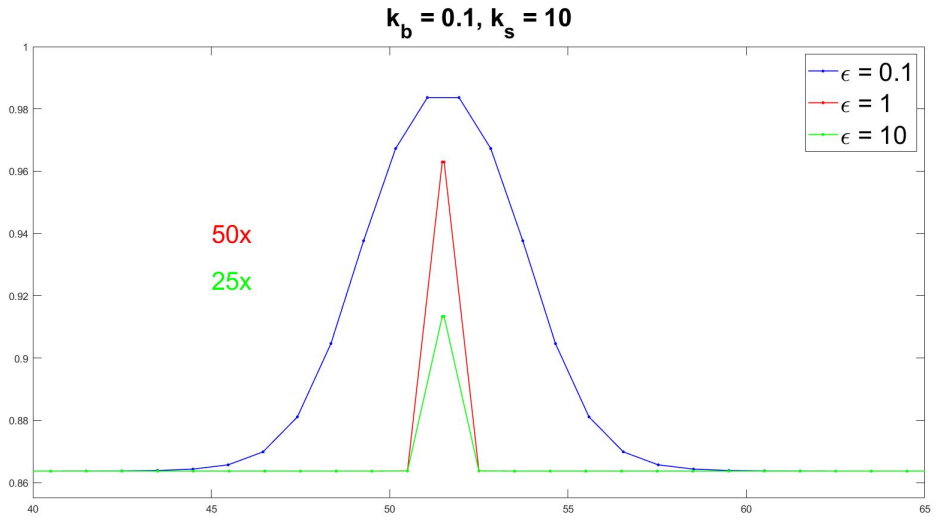

Figure 4.4: Here the red peak is amplified by a factor of 50, the green by 25.

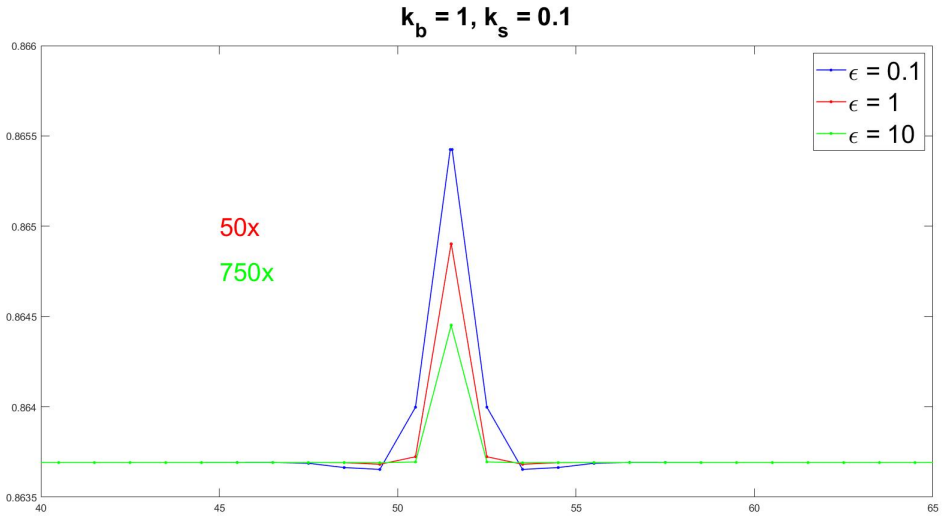

Figure 4.5: Here the red peak is amplified by a factor of 50, the green by 750.

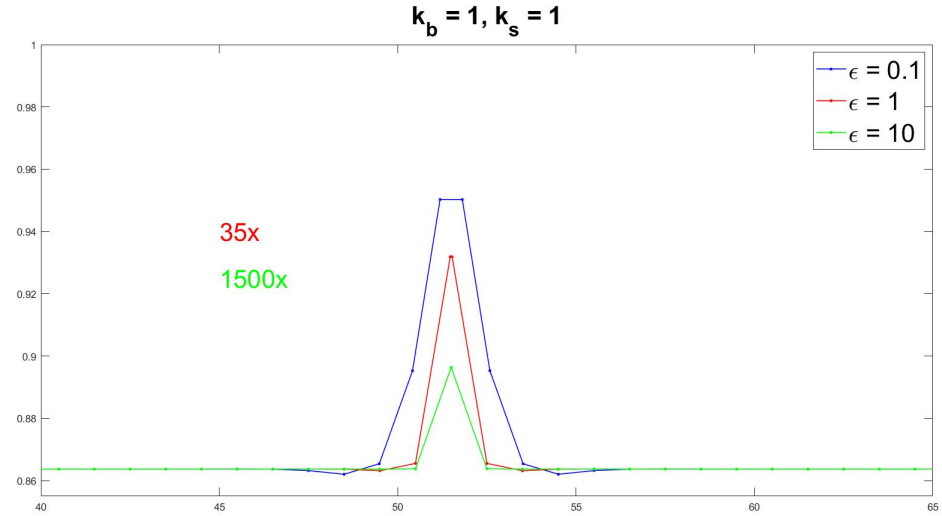

Figure 4.6: Here the red peak is amplified by a factor of 35, the green by 1500.

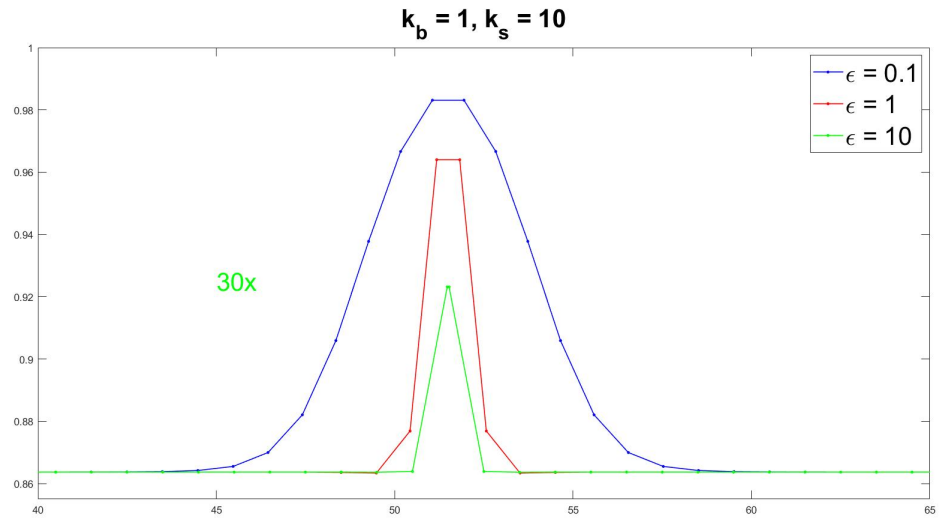

Figure 4.7: Here the green peak is amplified by a factor of 30.

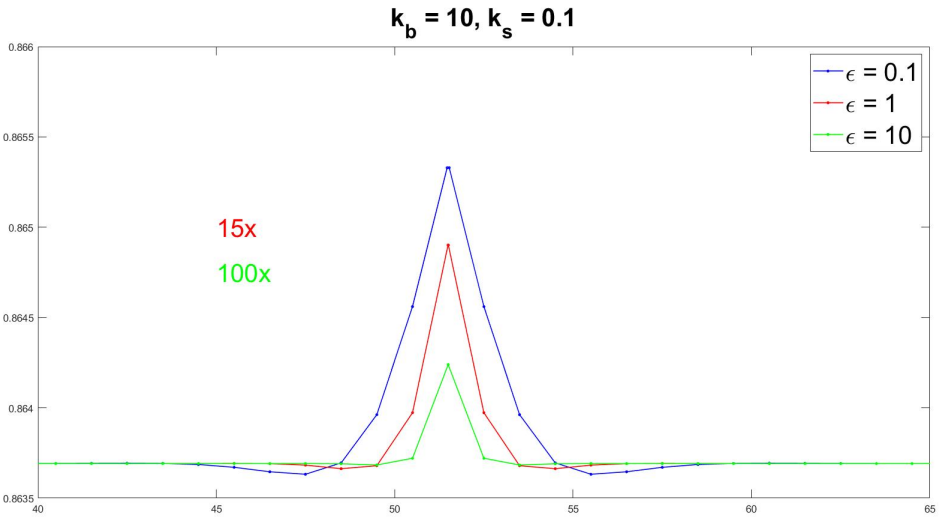

Figure 4.8: Here the red peak is amplified by a factor of 15, the green by 100.

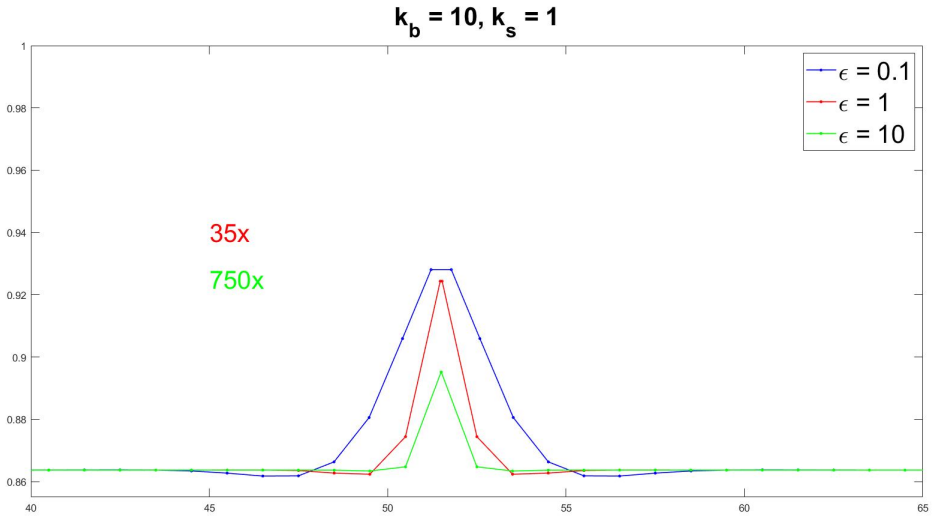

Figure 4.9: Here the red peak is amplified by a factor of 35, the green by 750.

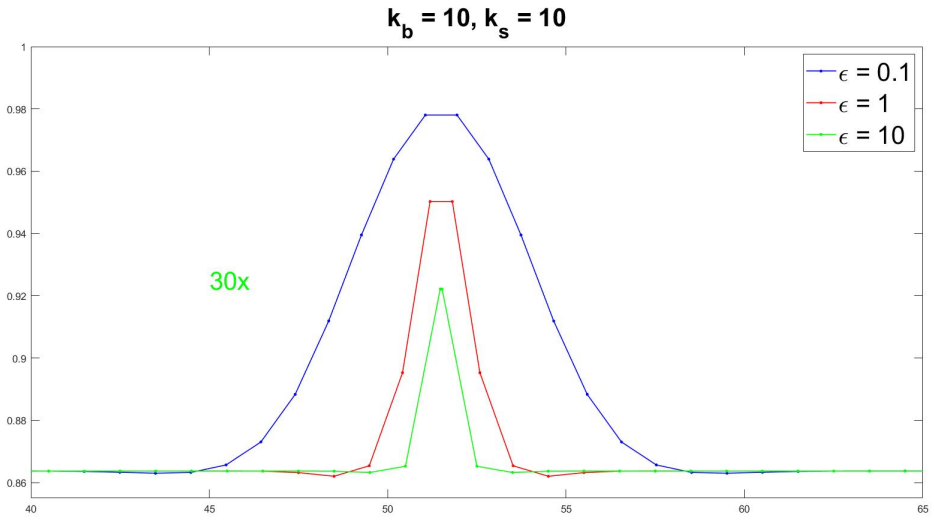

Figure 4.10: Here the green peak is amplified by a factor of 30.

As shown in each figure, the structure amplitudes decrease as the vdW forces become stronger (increasing ϵ). This behavior is seen clearly in figures 4.2 and 4.3, where the overall height of the peak decreases by a factor of over 1000 when $\epsilon = 10$. The elastic and bending forces affect the amplitude as well, although not as strongly. The structures tend to broaden as the elastic forces become stronger (increasing k_s). We can see the overall shape go from a sharp peak (figure 4.2) to one that is wider (figure 4.7). The vdW force has a similar affect, although not as strong.

Another interesting behavior we begin seeing is stationary oscillations (*i.e.* spatial modulations) in the structures. These oscillations are caused by an increase in the strength of the bending forces (increasing k_b). We see that this phenomenon is particularly prevalent when the bending forces are significantly stronger that the other forces (figure 4.8).

4.3 Example Study: Graphene

To examine a more realistic case, we will look at graphene. We will be running the same type of numerical simulation as in the previous subsection, but we will choose parameter values that are physically realistic for graphene. We can think of the top chain as the cross-section of a graphene layer and the bottom layer as the cross-section of a rigid graphite substrate. We will use the parameter values listed in table A.1. We set the number of atoms in the top layer to be one more than that of the bottom layer ($N = 101, M = 100$).

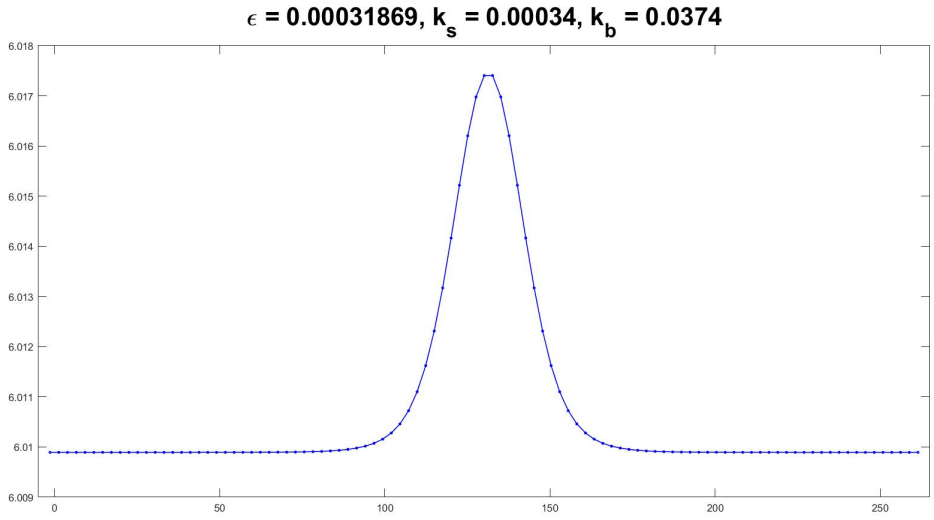

Figure 4.11: Equilibrium structure using parameters typical of a two-walled carbon nanotube.

In figure 4.11, we see that the peak is moderately round due to the vdW and elastic forces being almost equivalent. As the simulation contained one more atom in the top layer than the bottom layer, we see that, as expected, only one peak appears.

CHAPTER V

THERMAL EFFECTS ON EQUILIBRIUM STRUCTURES

We now incorporate temperature into our model to explore how temperature affects the equilibrium structures found in the previous chapter.

5.1 Analyzing Thermal Effects

To incorporate thermal effects into our system, we will use the Langevin model. This model was derived in chapter 3; see (3.2). Rewriting (3.2) but expressing the force as the negative gradient of the potential energy from equation (3.4), we get

$$m\frac{d^2\mathbf{r}_i}{dt^2} = -\nabla_{\boldsymbol{r}_i} U_i - \gamma\frac{d\mathbf{r}_i}{dt} + \sqrt{2\gamma k_B T}\boldsymbol{\eta}_i, \tag{5.1}$$

where all parameters and variables were defined in chapter 3. In particular, recall that T in the last term on the right-hand side of 5.1 is temperature.

We will be using the equilibrium structures obtained in chapter 4 as our initial condition. Temperature is a prescribed function of time. We start each simulation with $T = 0$. To avoid transient effects from the $T = 0$ initial condition, we will increase the temperature using a linear ramp to achieve a target temperature adiabatically. This equation for the temperature is given by

$$T(t) = at(1 - H(t-b)) + T_f H(t-b), \quad b = \frac{1}{a}T_f.$$

Here, we have a as the ramp rate, T_f is the final temperature achieved, and $H(t)$ is the Heaviside function. The temperature rises linearly according to the ramp rate. Once the time reaches the value b, the final temperature has been achieved and will remain constant at that temperature. In figure 5.1, we see an example of how the temperature function behaves.

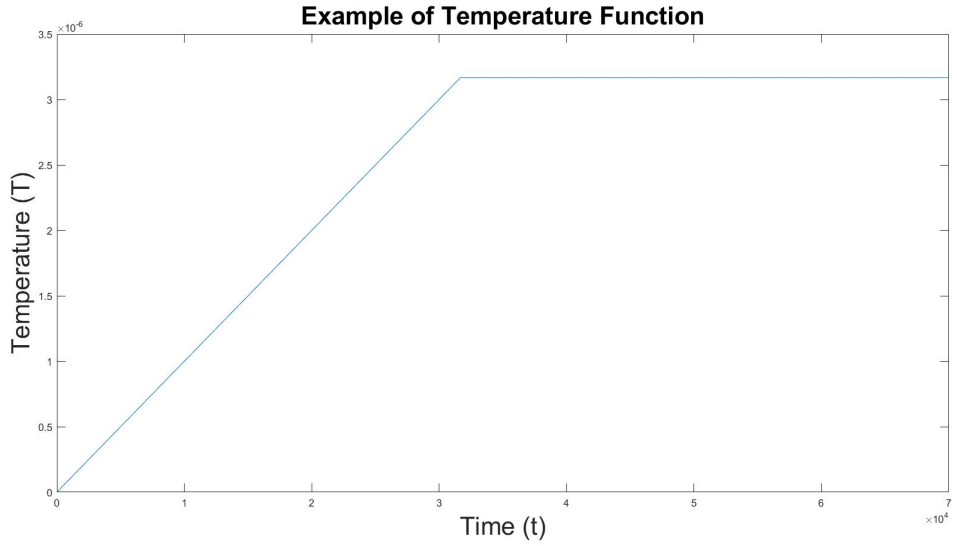

Figure 5.1: Example of the temperature function with a = 1e-10 and final temperature T_f = 3.167e-06 a.u. (1K).

For the van der Waals, stretching, and bending forces on the right-hand side of 5.1, we will use the same parameters as the zero-temperature graphene case, which are listed in table A.1. The vector $\boldsymbol{\eta}_i$ is random vector described by the Maxwell-Boltzmann distribution; see (2.27). The vector is calculated using Matlab's built-in function, randn. We will vary the final temperature in each simulation by a factor of 10. Once the final temperature has been achieved, the position of each atom will

be summed over a set number of time steps. Once the set number of time steps has passed, the average position will be calculated for each atom. Doing this gives us the average shape of the chain, which allows us to see how the temperature affects the overall structure.

5.2 Results from Thermal Effects

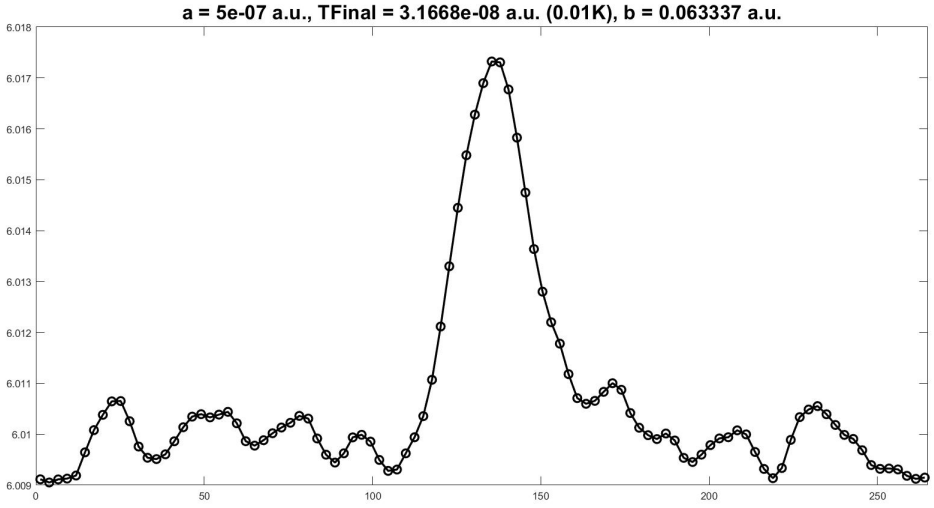

Figure 5.2: Typical structure observed for the final temperature T_f = 3.167e-8 a.u.(0.01K).

Results for the finite temperature case are shown. In figure 5.2, we see that the structure has begun to be affected by the thermal effects, although it remains stable (*i.e.* resembling its original configuration). In figure 5.3, we observe that the thermal fluctuations begin to approach a critical temperature where the structure would become unstable, although it still has not reached that state. In figure 5.4,

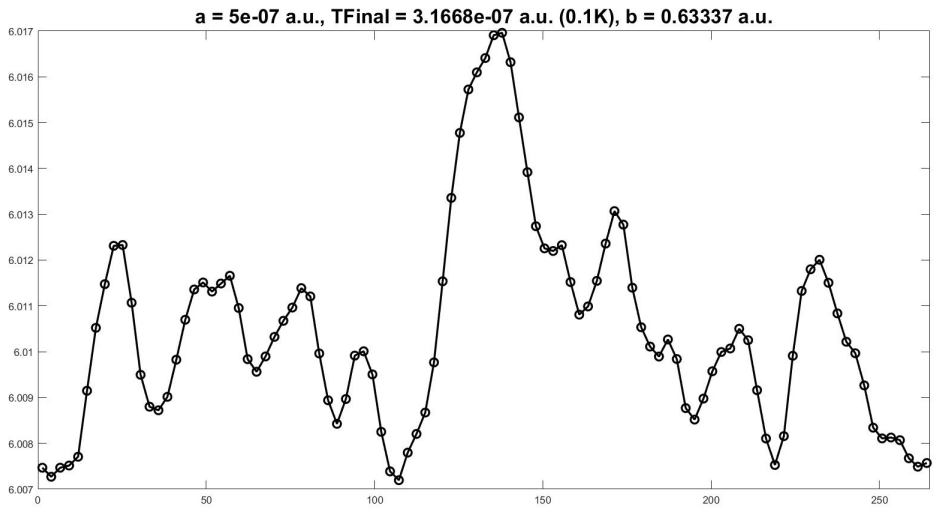

Figure 5.3: Typical structure observed for the final temperature T_f = 3.167e-7 a.u.(0.1K).

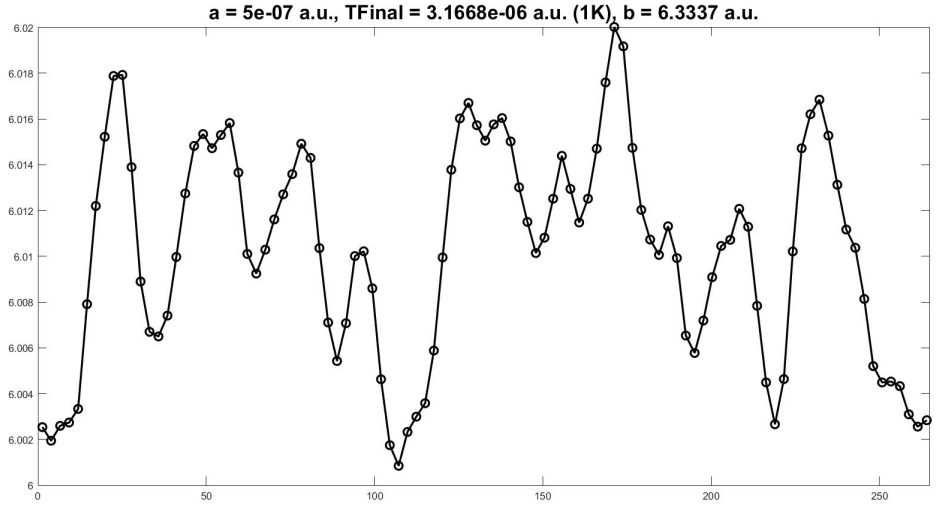

Figure 5.4: Typical structure observed for the final temperature T_f = 3.167e-6 a.u.(1K).

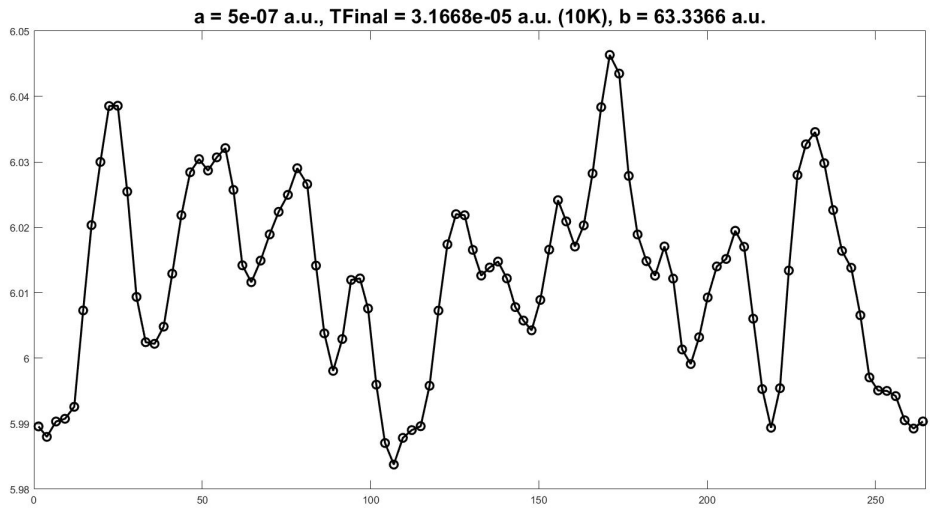

Figure 5.5: Typical structure observed for the final temperature T_f = 3.167e-5 a.u.(10K).

the structure has reached that critical temperature and has begun to destabilize; the original structure can only be partially made out as the destabilization occurs. Finally, in figure 5.5, the original structure is no longer visible and has destabilized. As seen in both figures 5.4 and 5.5, the structure will destabilize once the temperature gets too large. Therefore, there exists a critical temperature in which the stability of the structures will be compromised.

CHAPTER VI

INDENTATION SIMULATIONS

In this chapter we present simulations of the indentation of a graphene layer over a rigid substrate.

6.1 Model with Hole in Substrate

Our goal is to simulate an indenter pressing on a layer of graphene that is suspended over a substrate. The substrate has a gap or hole beneath the part of the layer on which the indenter is acting. In these simulations we exclude temperature effects. Thus, we can use the gradient flow model from chapter 4, which was derived as equation (3.15), as the starting point for this model. The action of the indenter is modeled by applying a constant force to a section of atoms on the free layer. We model the hole by removing atoms from the substrate.

We assume that there are N atoms on the free layer. We assume that there are M atoms in the middle of the layer are subject to the constant force. We let α denote the magnitude of the constant force. This force acts perpendicular to the substrate and pushes toward the substrate. To ensure that only the M selected atoms

are affected, we create for each i from 1 to N a vector, Φ_i, of zeros and ones as

$$\Phi_i = \begin{pmatrix} 0 \\ \\ \phi_i \end{pmatrix},$$

where

$$\phi_i = \begin{cases} 1 \quad \text{for} \quad \lfloor \frac{N}{2} \rfloor - \lfloor \frac{M}{2} \rfloor + 1 \quad \leq \quad i \quad \leq \quad \lfloor \frac{N}{2} \rfloor + \lceil \frac{M}{2} \rceil \\ 0 \qquad\qquad\qquad\qquad otherwise \end{cases}.$$

Thus we can now add our constant force term into equation (3.15) and get

$$\frac{d\boldsymbol{r}_i}{dt} = -\frac{1}{\gamma} \nabla_{\boldsymbol{r}_i} U_i - \alpha \Phi_i. \tag{6.1}$$

For these simulations, the use of the periodic boundary conditions is not desired, so the ghost atoms in the calculations of the forces are not used. A uniform chain, whose height will be varied, will be used as an initial condition. The stopping criteria for the simulations is the same that was used in chapter 4. To determine when equilibrium has been attained, we set a numerical tolerance. After a set number of time steps, the overall absolute value of the displacement of each atom, from its previously checked position, will be summed and if the total is smaller than the tolerance, the system will be deemed to be equilibrated. The simulation is ended, and the final position will be the equilibrium structure. Also, the free layer will be deemed as passing through the substrate if any atom's y-position falls below zero. Any atom's y-position falling below zero will not be deemed as a stopping condition.

6.2 Deflection From Constant Force

We explore how far the atoms in the free chain get pushed downwards as a result of the constant force. We execute this by varying the strength of the constant force, α, and for each atom on the free layer computing the difference between that atom's initial y-coordinate and its final y-coordinate. The maximum of these differences over the whole layer is what we refer to as the max deflection. For our experiment, we fix the total number of atoms in the free chain to fifty, $N = 50$, and the number of atoms affected by the constant force to four, $M = 4$.

We will use two different sets of parameters. The first will be that of the graphene case. We will set the substrate hole to 25.398 bohr, four times the graphene vdW radius. All other parameters, such as the natural length of the elastic bond connecting the neighboring atoms in the free chain, are listed in table A.1. We will also begin with a uniform chain that has a height of 5.71455 bohr, which is 90% of the graphene vdW radius. For the second set of parameters we use a variation of the graphene parameters. These parameters are used to see differences in the deflection compared to the graphene case. We will set the substrate hole to 10.12892 bohr, four times the non-graphene vdW radius. All other parameters are listed in table A.2. We will begin this test with a uniform chain that has a height of 2.279 bohr, 90% of the vdW radius used in these simulations.

Figures 6.1 and 6.2 shows the results of our experiments. Here we see that points have one of two colors, blue or red. If a point is blue, it means that no atoms

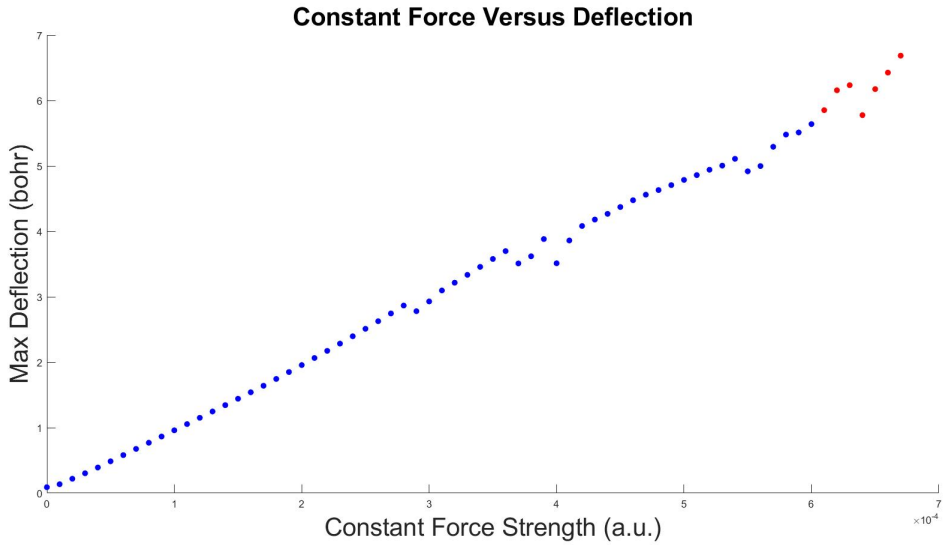

Figure 6.1: Resulting graph of constant force versus deflection simulation with graphene parameters.

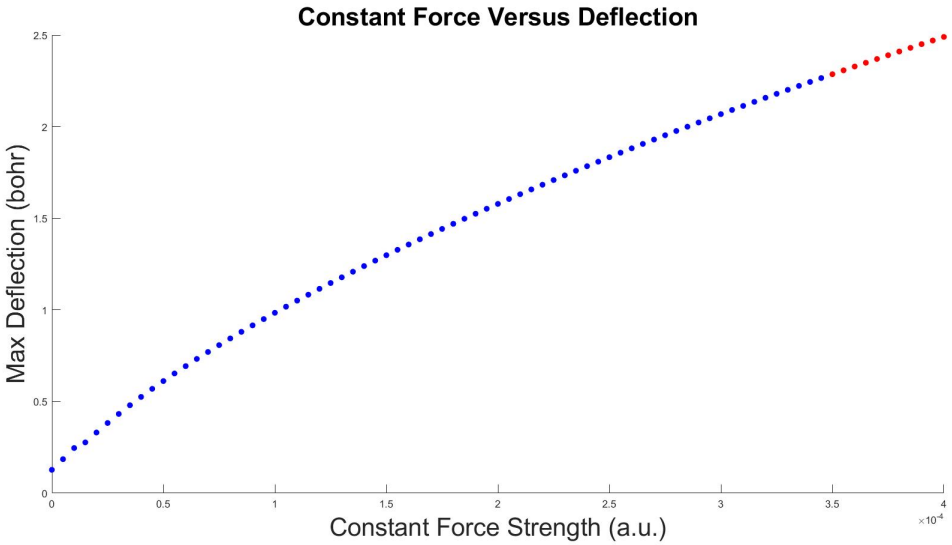

Figure 6.2: Resulting graph of constant force versus deflection simulation with the parameters in table A.2.

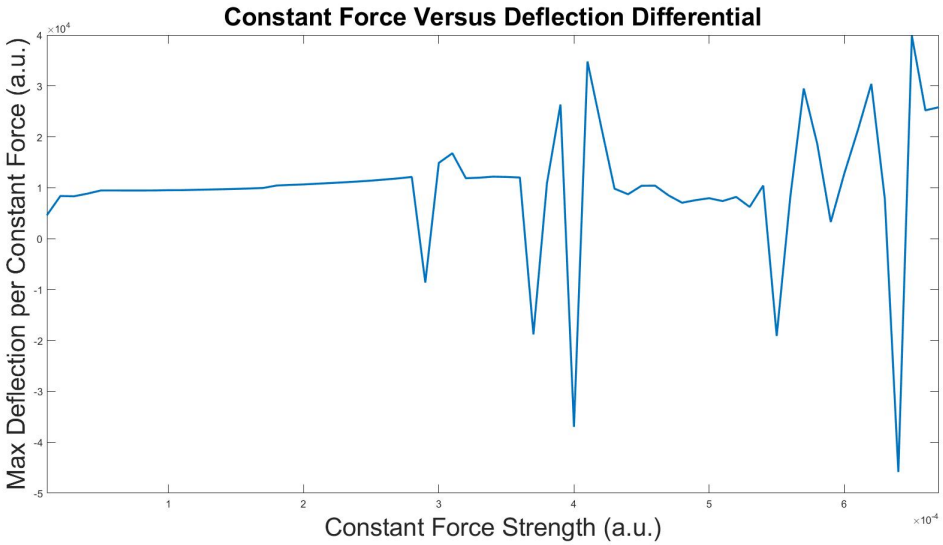

Figure 6.3: Differential graph of constant force versus deflection simulation with graphene parameters.

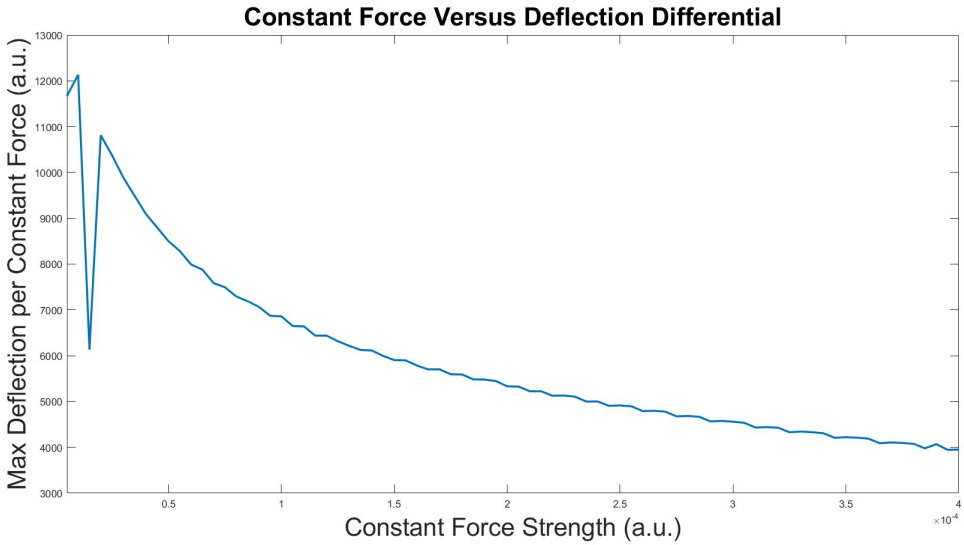

Figure 6.4: Differential graph of constant force versus deflection simulation with the parameters in table A.2.

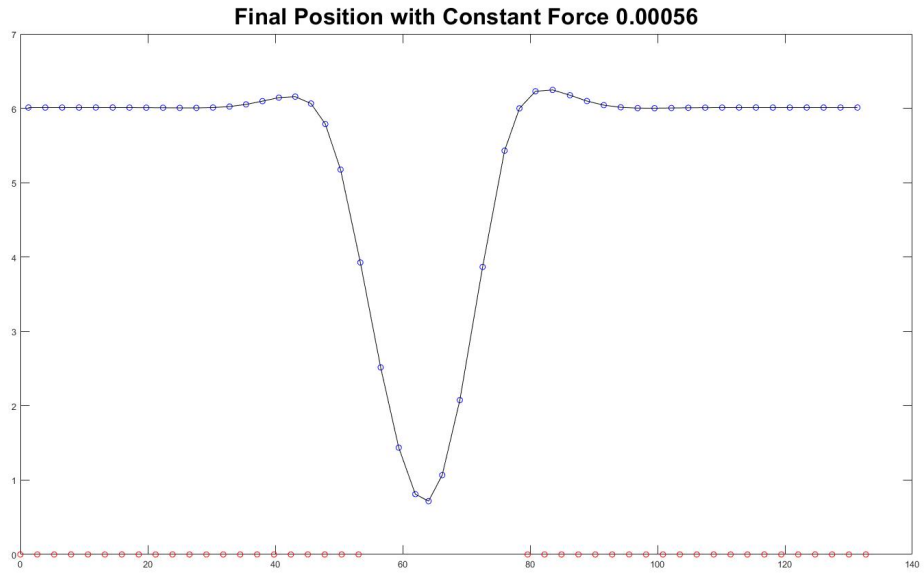

Figure 6.5: A final position in which the chain did not pass through the substrate. (graphene)

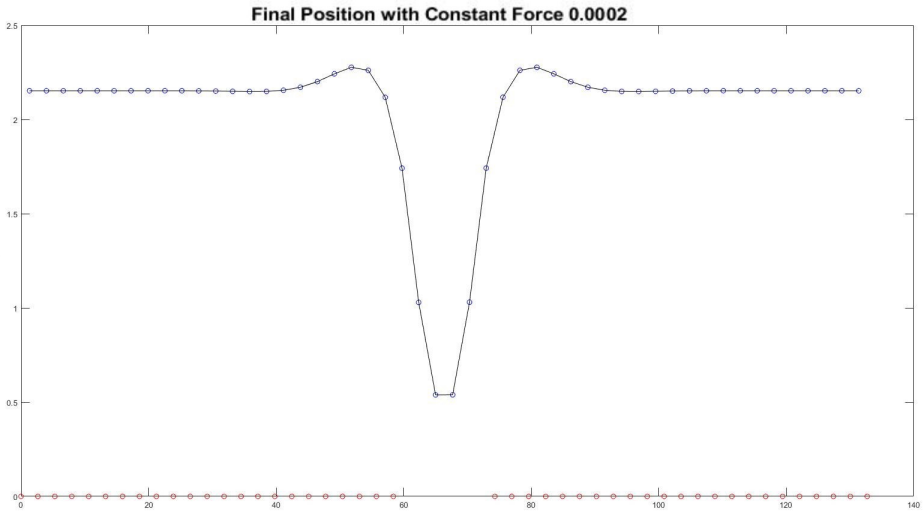

Figure 6.6: A final position in which the chain did not pass through the substrate. (non-graphene)

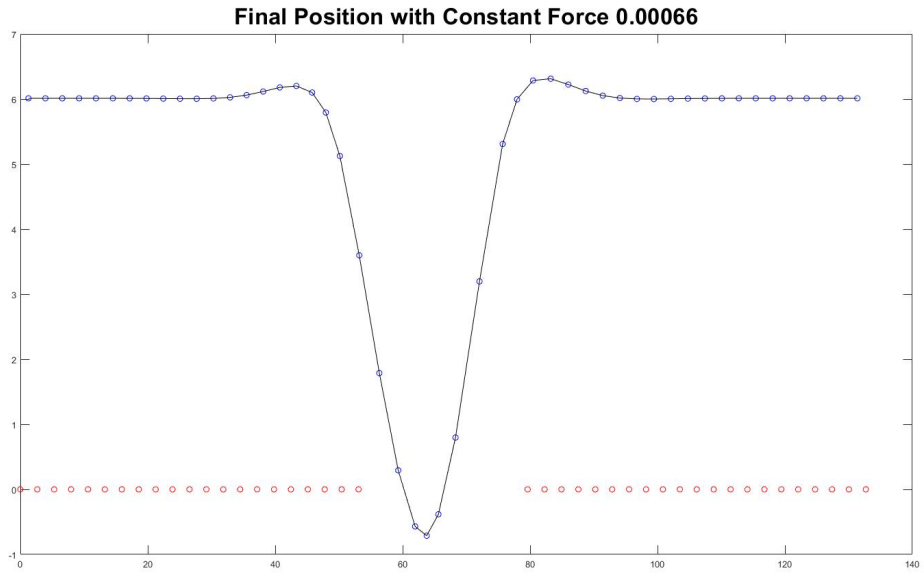

Figure 6.7: A final position in which the chain did pass through the substrate. (graphene)

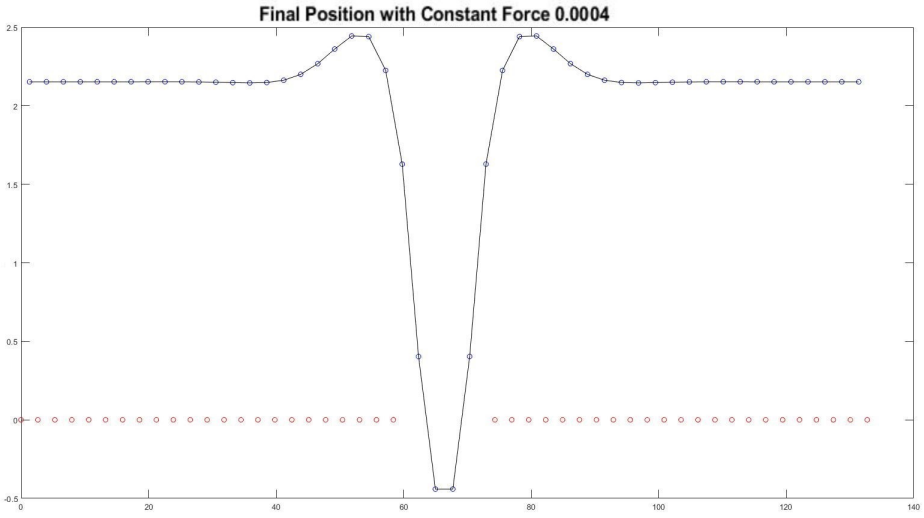

Figure 6.8: A final position in which the chain did pass through the substrate. (non-graphene)

passed through the hole in the substrate, while red signifies that at least one atom did. Figures 6.3 and 6.4 show the numerical differentials of 6.1 and 6.2, which are numerical derivatives of the curves in figures 6.1 and 6.2. In figures 6.5 and 6.6 we see the final positions for both parameter sets in which the top layer did not cross through the substrate. In figures 6.7 and 6.8 we see the final positions for both parameters sets in which the top layer did cross through the substrate.

From figure 6.1, we see that, for the graphene parameters, the overall shape of the deflection is linear. This linear behavior is more apparent in the plot of the corresponding differential; see figure 6.3. The differential, through the noise, is almost constant, implying linear deflection. From figure 6.2, we see that, for the second set of parameters, the overall shape appears to follow the shape of a square root function, but slightly more linear. We see that the differential, figure 6.4, confirms this. The rate of change decreases rapidly initially but becomes more constant at the end. Overall, both behaviors describe what we expect. As the constant force increases, the max deflection increases as well.

6.3 Equilibriums with Varying Lengths

We execute another parameter study to explore the effects of varying the distance between atoms in the substrate, h_1, the natural length of the bonds in the free chain, h_2, and the vdW radius, σ. We will use the set $\{1,2,3\}$ as the values of our parameters. All other parameters will be the same as that of the non-graphene

case listed in table A.2. The constant force will also be set to 2e-4 a.u. (force) and the hole in the substrate will be set to 4 bohr for all numerical experiments.

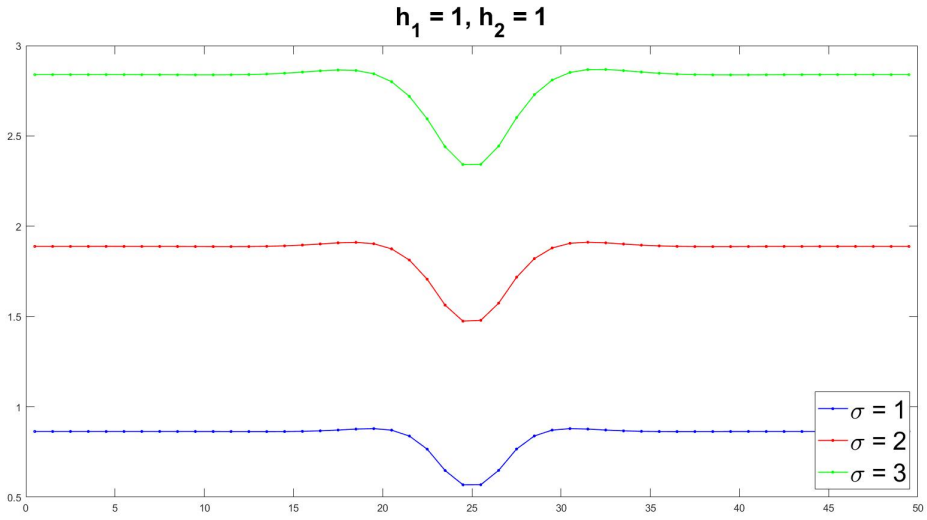

Figure 6.9: Equilibrium structures in the (h_1, h_2, σ) space.

In every figure, we can see that as the value of σ goes up, so does the entire chain. This behavior is expected as the substrate repels the top chain to a further distance determined by σ. As h_2 increases, we see that the depth of the valley increases, figure 6.14 best demonstrates this. As h_2 is the length of the bonds in the top chain, the larger its value, the farther it will repel its neighbors. That, combined with the constant force, pushes the valley farther down. If the value of h_1 is small, it is more difficult for atoms to pass through the substrate. We see this behavior prominently in figure 6.11 in which no atoms crossed through the substrate,

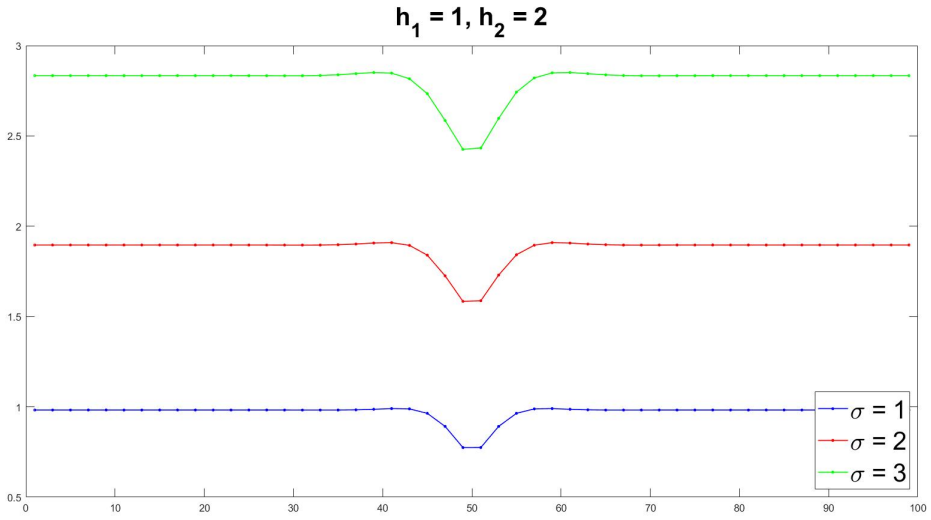

Figure 6.10: Equilibrium structures in the (h_1, h_2, σ) space.

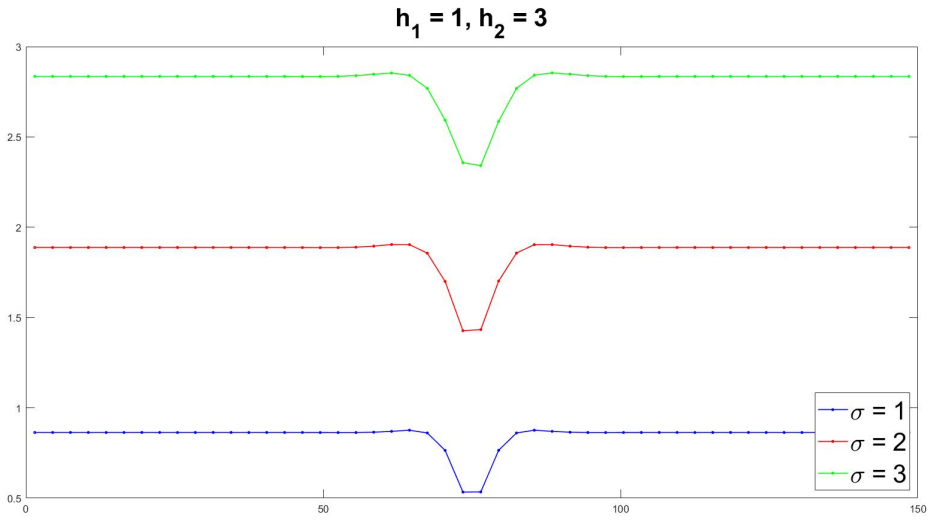

Figure 6.11: Equilibrium structures in the (h_1, h_2, σ) space.

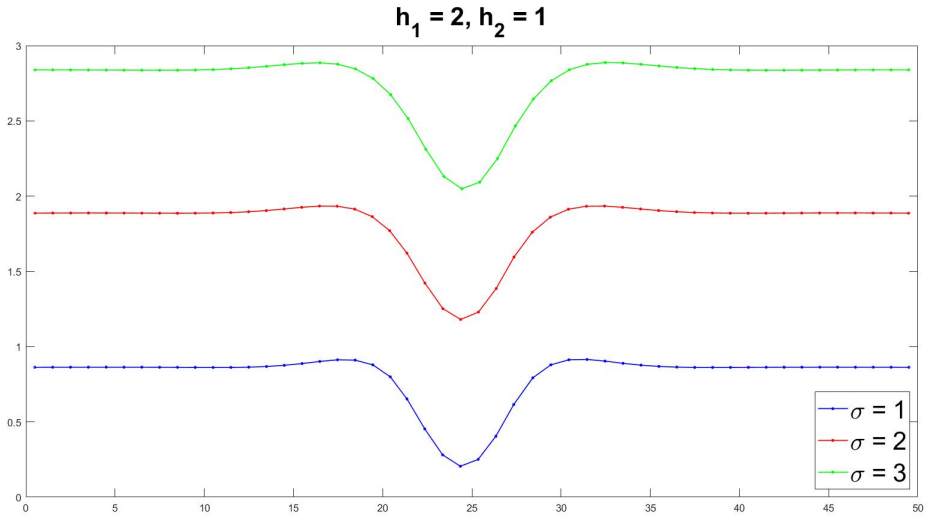

Figure 6.12: Equilibrium structures in the (h_1, h_2, σ) space.

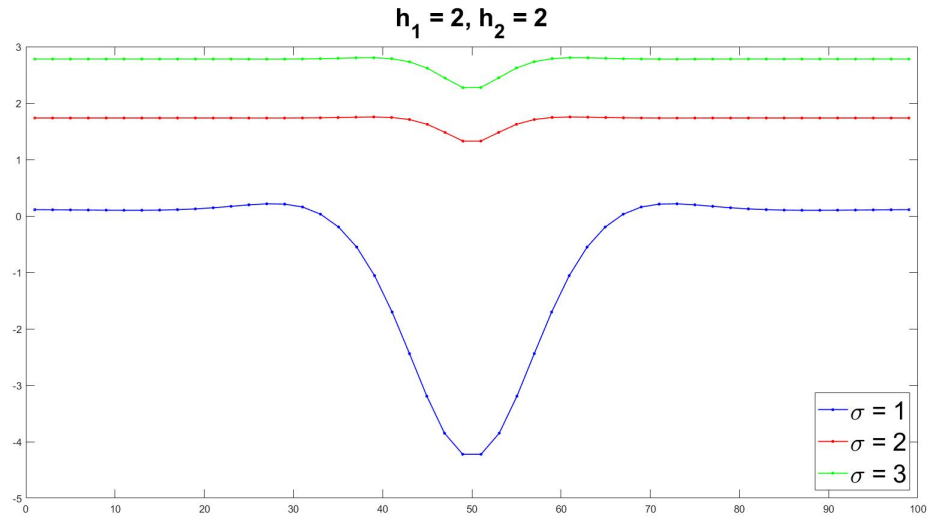

Figure 6.13: Equilibrium structures in the (h_1, h_2, σ) space.

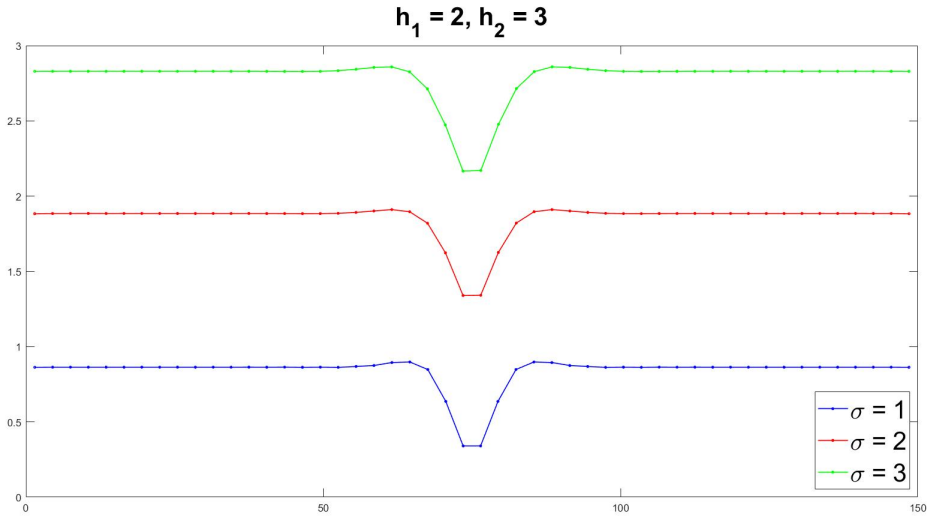

Figure 6.14: Equilibrium structures in the (h_1, h_2, σ) space.

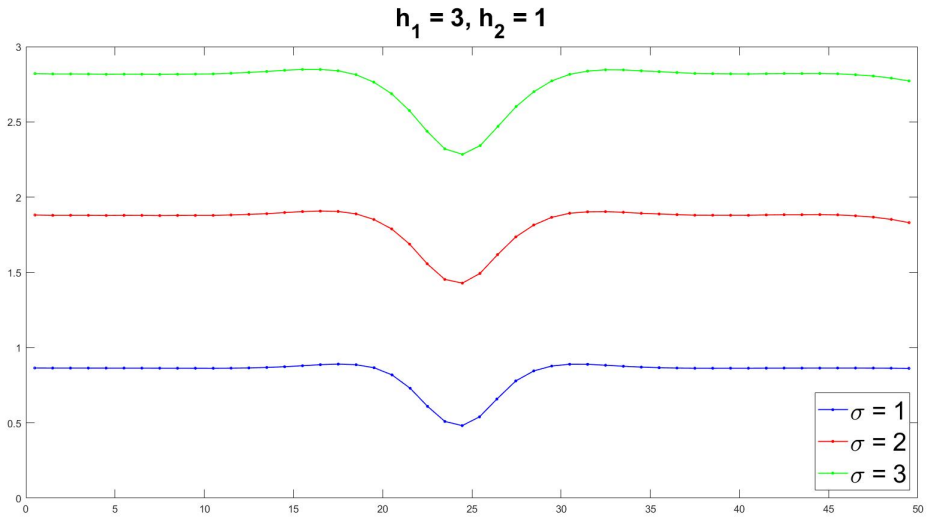

Figure 6.15: Equilibrium structures in the (h_1, h_2, σ) space.

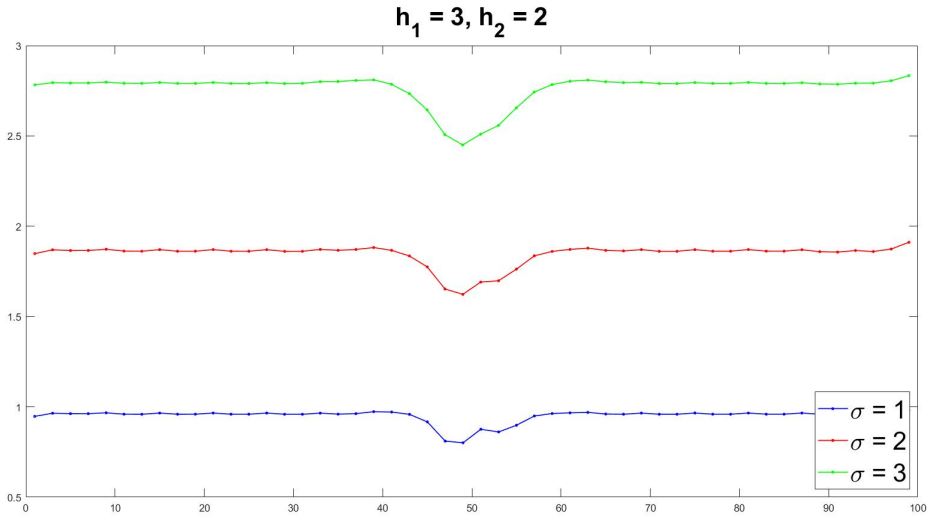

Figure 6.16: Equilibrium structures in the (h_1, h_2, σ) space.

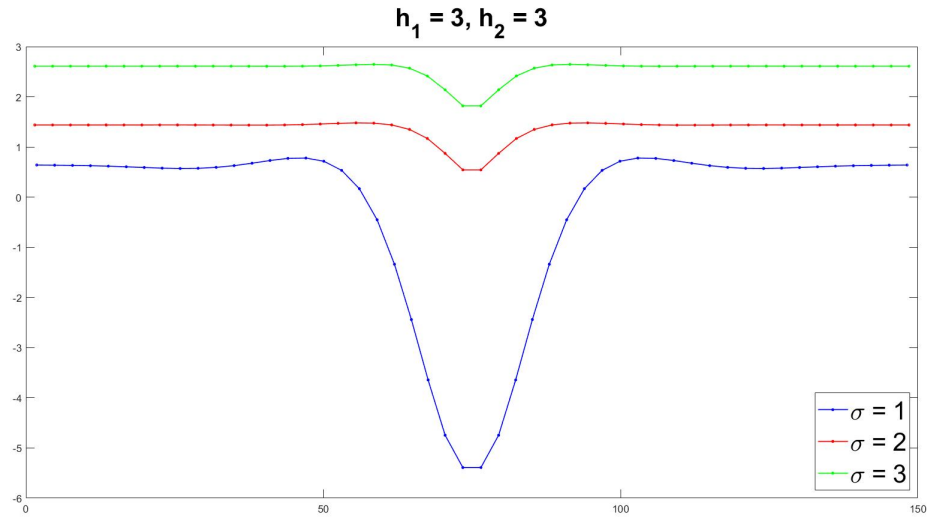

Figure 6.17: Equilibrium structures in the (h_1, h_2, σ) space.

as opposed to figures 6.14 and 6.17 where the top layer had some atoms pass through the substrate.

In figures 6.13 and 6.17, we see that the simulations where $\sigma = 1$, the final configurations crossed through the substrate. With the substrate hole size being 4 bohr, atoms can fit through the hole without being repelled upwards.

6.4 Pass Through Substrate

Having a hole in the substrate allows from atoms to cross through the substrate. We have seen some atoms in the top layer cross through the substrate, see figure 6.13 or 6.17, but we desire to see if there exists a set of values for each force in which the entire top layer crosses through the hole in the substrate. We use the parameters in table A.2, expect that we vary the strengths of the vdW interaction, stretching force, bending force, and the constant force. We also fix the hole in the substrate to 15.92 bohr, or six times the value of h_1.

After experimenting with different strengths of each force, we discovered a set of values in which the top layer completely crosses through the substrate. We have ϵ = 2.04e-4 hartree for the vdW force, k_s = 24.09 a.u.(pressure) for the stretching, k_b = 0.72 hartree for the bending, and $\alpha = 0.7$ a.u.(force) for the constant force.

As seen in figure 6.21, it is possible for the top layer to cross completely through the substrate. The strength of the stretching force, k_s, is much larger than that commonly found in graphene. Although we are able to simulate this complete

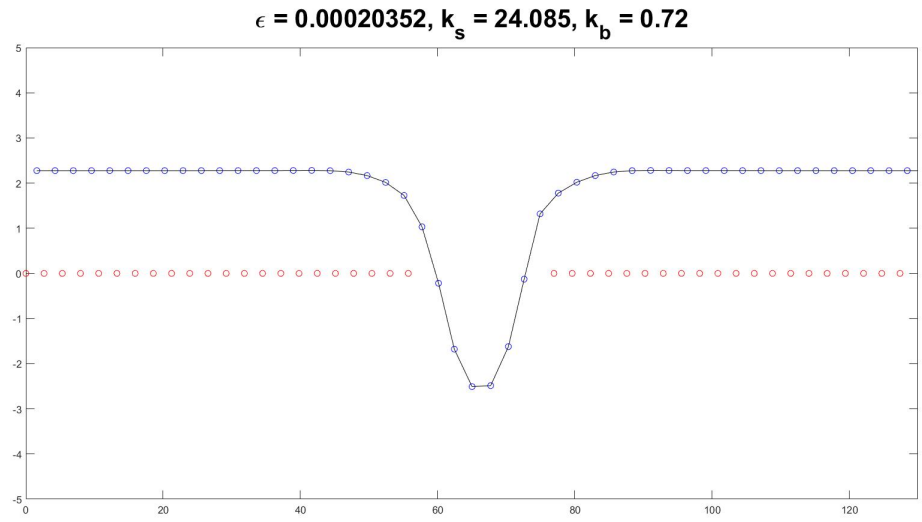

Figure 6.18: Top layer (blue) begins to pass through the substrate (red).

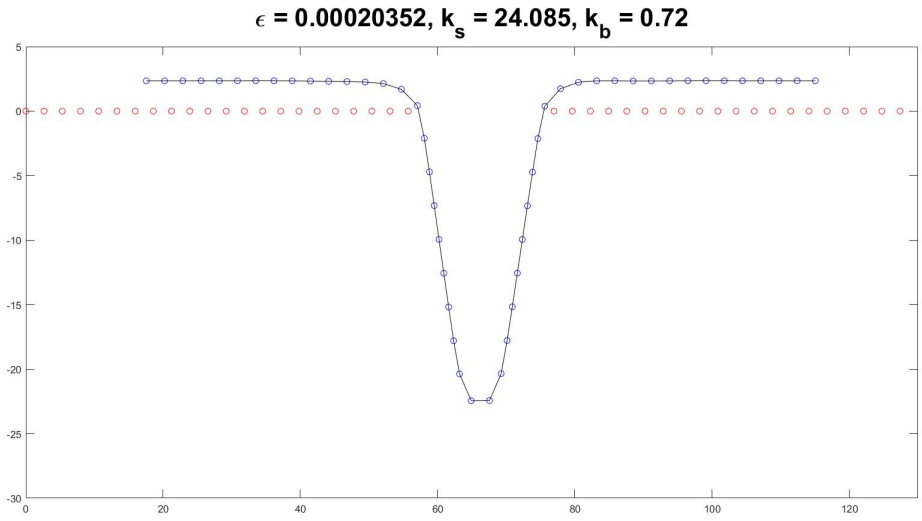

Figure 6.19: Top layer (blue) passed halfway through the substrate (red).

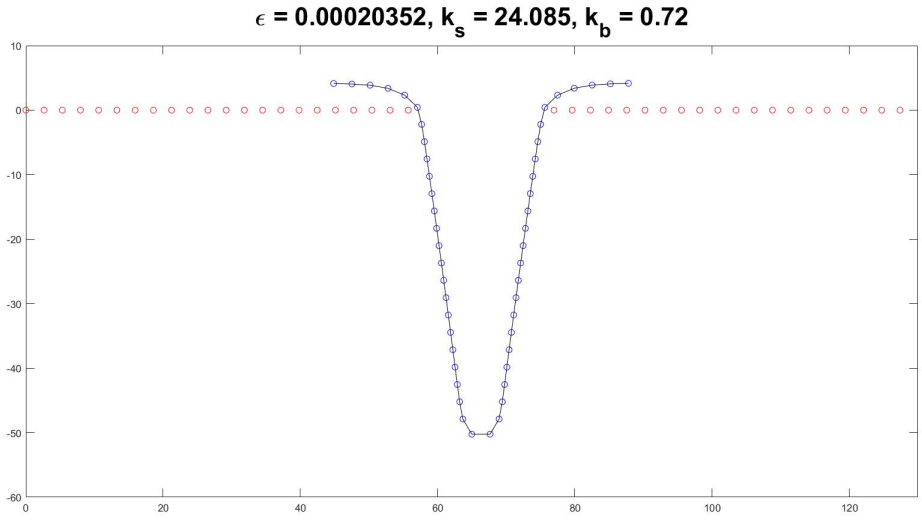

Figure 6.20: Top layer (blue) has nearly passed through the substrate (red).

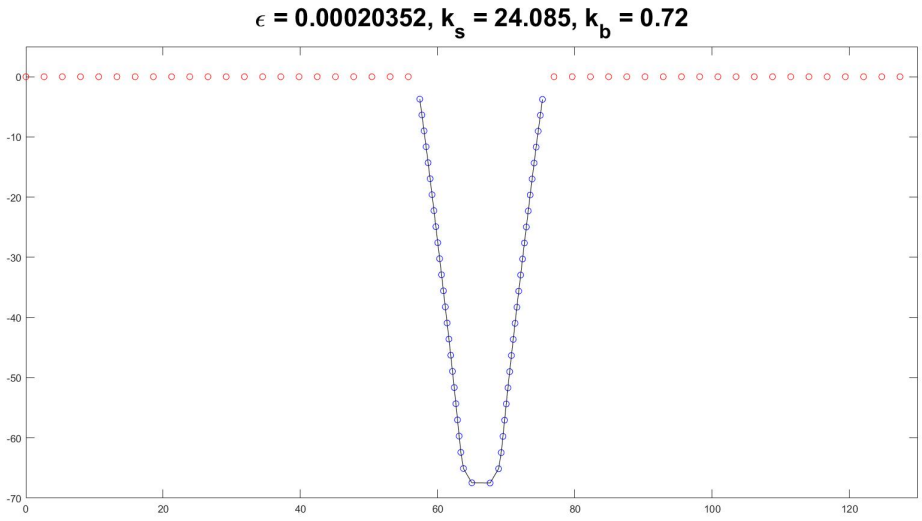

Figure 6.21: Top layer (blue) completely passed through the substrate (red).

crossing through of the substrate numerically, it may not be physically possible without a significantly large substrate hole.

CHAPTER VII

DISCUSSION AND CONCLUSION

Nanostructures have become an extensively studied topic that continues today to attract a deal of scientific interest. Although researchers develop and study different nanostructures in laboratories, mathematical modeling and numerical methodologies have been useful tools in furthering these experimental studies. Below we briefly review the results from the numerical experiments presented in this thesis. We also briefly discuss some related future work that could be done.

7.1 Results from Numerical Experiments

We explored the effects of different strengths of forces and how they create various structures. The equilibrium structures were drastically affected by the values of all three force strengths. The amplitude and the width of the resulting structures were shown to be affected mostly by the strengths of the vdW and elastic forces. We also observed that the bending forces induced oscillatory structures. After running a numerical experiment with parameter values consistent with the properties of graphene, we saw that these results were consistent with the results of the larger parameter study in the sense that the equilibrium structure followed a more oscilla-

tory structure, as the bending force was stronger than that of the vdW and bonding energies.

We also examined how the incorporation of temperature and how thermal fluctuations affect equilibrium structures. Once we added finite temperature into the model, we were able to see the thermal fluctuations destabilize the equilibrium structures.

We also modified our model to describe the indentation of a graphene layer. This model included placing a hole in the rigid substrate and a constant force pushing down on a fixed number of atoms in the top layer. The resulting equilibrium structures exhibited valleys in the top layer. As the strength of the constant force increases, the maximum deflection, which measured the depth of the valley, also increases. The length of the vdW radius increases the distance between the top layer and the substrate. As the length of the bonds in the top layer increases the depth of the valley in the top layer also increases. The ability for atoms in the top layer to cross through the substrate becomes more difficult as the distance between atoms in the rigid substrate decreases. When the parameters are chosen properly, it is possible for the top layer to fully pass through the hole in the substrate.

7.2 Future Work

Although extensive work was done to create the numerical experiments and acquire results, more experiments are still needed. These include using different parameters based on different materials to get more equilibrium structures that can

also be examined with thermal effects incorporated. The use of different parameters in both the study of deflection and lengths in the model that contains a hole in the substrate also is needed to further draw conclusions.

One aspect that is not discussed in this thesis that would be explored is the inclusion of temperature in the model with a hole in the substrate. Another area that was not explored was the creation of a model that contained more than one hole in the substrate. Allowing for more holes and varying their locations requires extensive work but would be beneficial. After examining the equilibrium structures with multiple holes in the substrate, the addition of temperature again would be experimented with. Allowing for the chain of atoms to include atoms of different elements is also desired as not all materials are made of one element. Lastly, expanding all models to include a third dimension so that it more accurately depicts the real world would be implemented for more experimentation.

7.3 Conclusion

Nanostructures have been extensively studied. Various properties and applications have already been examined. With that in mind, there are still many properties that are yet to be studied and some that are yet to be discovered. With the abundance of combinations of materials and geometries, nanostructures hold great promise for novel applications and hence will continue to be extensively studied.

BIBLIOGRAPHY

[1] Anqi Zhang, G. Zheng, and Charles Lieber. *Nanowires: Building Blocks for Nanoscience and Nanotechnology.* NanoScience and Technology. Switzerland: Springer, 2016.

[2] G. Dresselhaus, M. S. Dresselhaus, and A. Jorio. *Carbon nanotubes. [electronic resource] : advanced topics in the synthesis, structure, properties, and applications.* Topics in applied physics: v. 111. Berlin ; New York : Springer, 2008.

[3] Zhong Lin Wang. Zinc oxide nanostructures: growth, properties and applications. *Journal of Physics: Condensed Matter*, 16(25):R829, 2004.

[4] X. W. Lou, Y. Wang, C. Yuan, J. Y. Lee, and L. A. Archer. Template-Free Synthesis of SnO2 Hollow Nanostructures with High Lithium Storage Capacity. *Advanced Materials*, 18(17):2325–2329, 2006.

[5] L.-S. Zhong, J.-S. Hu, H.-P. Liang, A.-M. Cao, W.-G. Song, and L.-J. Wan. Self-Assembled 3d Flowerlike Iron Oxide Nanostructures and Their Application in Water Treatment. *Advanced Materials*, 18(18):2426–2431, 2006.

[6] Aurangzeb Khan. *Synthesis, Characterization and Luminescence Properties of Zinc Oxide Nanostructures.* Ohio University / OhioLINK, 2006.

[7] Madhuri Sharon and Maheshwar Sharon. *Graphene : an introduction to the fundamentals and industrial applications.* Advanced material series. Hoboken, New Jersey : Wiley, 2015.

[8] E. L. Wolf. *Graphene : a new paradigm in condensed matter and device physics.* Oxford : Oxford University Press, 2013.

[9] Marcin Mucha-Kruczyski. *Theory of bilayer graphene spectroscopy. [electronic resource].* Springer theses. Berlin : Springer, [2013], 2013.

[10] Wei Mu, Yifeng Fu, Shuangxi Sun, Michael Edwards, Lilei Ye, Kjell Jeppson, and Johan Liu. Controllable and fast synthesis of bilayer graphene by chemical vapor deposition on copper foil using a cold wall reactor. *Chemical Engineering Journal*, 304:106–114, November 2016.

[11] Bor-Luen Huang, Chih-Piao Chuu, and Ming-Fa Lin. Asymmetry-enriched electronic and optical properties of bilayer graphene. *Scientific Reports, Vol 9, Iss 1, Pp 1-12 (2019)*, (1):1, 2019.

[12] N.M.R. Peres. The electronic properties of graphene and its bilayer. *Vacuum*, 83:1248–1252, January 2009.

[13] A. Moreno-Brcenas, J. F. Perez-Robles, Y. V. Vorobiev, N. Ornelas-Soto, A. Mexicano, and A. G. Garca. Graphene Synthesis Using a CVD Reactor and a Discontinuous Feed of Gas Precursor at Atmospheric Pressure. *Journal of Nanomaterials*, pages 1–11, March 2018.

[14] Luo Wen-Gang, Wang Hua-Feng, Cai Kai-Ming, Han Wen-Peng, Tan Ping-Heng, Hu Ping-An, and Wang Kai-You. Synthesis of Homogenous Bilayer Graphene on Industrial Cu Foil. *CHINESE PHYSICS LETTERS*, 31(6), June 2014.

[15] Y. Xia, P. Yang, Y. Sun, Y. Wu, B. Mayers, B. Gates, Y. Yin, F. Kim, and H. Yan. One-Dimensional Nanostructures: Synthesis, Characterization, and Applications. *Advanced Materials*, 15(5):353–389, 2003.

[16] James E. Morris and Krzysztof Iniewski. *Graphene, Carbon Nanotubes, and Nanostructures: Techniques and Applications.* Devices, Circuits, and Systems. Boca Raton, FL : CRC Press, 2013.

[17] Yunxiang Bai, Rufan Zhang, Xuan Ye, Zhenxing Zhu, Huanhuan Xie, Boyuan Shen, Dali Cai, Bofei Liu, Chenxi Zhang, Zhao Jia, Shenli Zhang, Xide Li, and Fei Wei. Carbon nanotube bundles with tensile strength over 80 GPa. *NATURE NANOTECHNOLOGY*, 13(7):589–+, July 2018.

[18] Banafsheh Sajadi, Simon van Hemert, Behrouz Arash, Pierpaolo Belardinelli, Peter G. Steeneken, and Farbod Alijani. Size- and temperature-dependent bending rigidity of graphene using modal analysis. *CARBON*, 139:334–341, November 2018.

[19] Anton Kuzyk, Robert Schreiber, Zhiyuan Fan, Gnther Pardatscher, Eva-Maria Roller, Alexander Hgele, Friedrich C. Simmel, Alexander O. Govorov, and Tim Liedl. DNA-based self-assembly of chiral plasmonic nanostructures with tailored optical response. *Nature*, 483(7389):311–314, March 2012.

[20] Huo Xu, Shuxin Zhang, Changhe Ouyang, Zhenmeng Wang, Dong Wu, Yiyun Liu, Yifan Jiang, and Zai-Sheng Wu. DNA nanostructures from palindromic rolling circle amplification for the fluorescent detection of cancer-related microRNAs. *Talanta*, 192:175–181, January 2019.

[21] Reza Karimi Shervedani, Fatemeh Yaghoobi, Mostafa Torabi, Fatemeh Rahnemaye Rahsepar, and Marzieh Samiei Foroushani. Controlled synthesis of mixed molecular nanostructures from folate and deferrioxamine-Ga(III) on gold and tuning their performance for cancer cells. *Bioelectrochemistry (Amsterdam, Netherlands)*, 122:149–157, August 2018.

[22] DeShan Bin, Yunming Li, YongGang Sun, ShuYi Duan, Yaxiang Lu, Jianmin Ma, AnMin Cao, YongSheng Hu, and LiJun Wan. Structural Engineering of Multishelled Hollow Carbon Nanostructures for HighPerformance NaIon Battery Anode. *Advanced Energy Materials*, 8(26):1–1, September 2018.

[23] Michael P. Allen. Introduction to Molecular Dynamics Simulation. In Gustav-Stresemann-Institut e.V. fr bernationale Bildung und Europische Zusammenarbeit, John von Neumann-Institut fr Computing, Johannes Gutenberg-Universitt Mainz, Max-Planck-Institut fr Biophysikalische Chemie, and Max-Planck-Institut fr Polymerforschung, editors, *Computational Soft Matter: From Synthetic Polymers to Proteins; Winter School, 29 February - 6 March 2004, Gustav-Stresemann-Institut, Bonn, Germany. 2: Lecture Notes*, number 23 in NIC series. NIC, Jlich, 2004.

[24] Emmanuel Rivera, Liam Stanton, Malena Español, Dmitry Golovaty, and J. Patrick Wilber. Móire Patterns and Thermal Fluctuations in Interacting Monolayers. Technical report, Lawrence Livermore National Laboratory, September 2017.

[25] Michael Fowler. Brownian Motion. University of Virginia.

[26] J. Richard Elliott and Carl T. Lira. *Introductory Chemical Engineering Thermodynamics*. Upper Saddle River, NJ : Prentice Hall PTR, second edition, 2012.

[27] Gustav Kirchhoff. Vorlesungen uber Mechanik. In *Lectures on Mechanics*, pages 378–380.

[28] Albert Einstein. On the Motion of Small Particles Suspended in Liquids at Rest Required by the Molecular-Kinetic Theory of Heat. pages 1–7.

[29] Fatmir Qirezi. From Stochastic to Deterministic Langevin Equation, 2009.

[30] Sir George Gabriel Stokes. MATHEMATICAL AND PHYSICAL PAPERS. page 427.

[31] Don S. Lemons and Anthony Gythiel. Paul Langevins 1908 paper On the Theory of Brownian Motion [Sur la thorie du mouvement brownien, C. R. Acad. Sci. (Paris) **146** , 530533 (1908)]. *American Journal of Physics*, 65(11):1079–1081, November 1997.

[32] Jens Timmer. Brownian Motion and Langevin Equations. University of Freiburg.

[33] Loup Verlet. Computer "Experiments" on Classical Fluids. I. Thermodynamical Properties of Lennard-Jones Molecules. *Physical Review*, 159(1):98–103, July 1967.

[34] William C. Swope, Hans C. Andersen, Peter H. Berens, and Kent R. Wilson. A computer simulation method for the calculation of equilibrium constants for the formation of physical clusters of molecules: Application to small water clusters. *The Journal of Chemical Physics*, 76(1):637–649, January 1982.

APPENDIX

PARAMETER VALUES

Table A.1: Graphene Parameters in Atomic Units

Name	**Variable**	**Value**
vdW Strength	ω	3.18692e-4 hartree
Bond Strength	k_s	3.4e-4 a.u. (pressure)
Bending Strength	k_b	3.74e-2 hartree
vdW Radius	σ	6.3495 bohr
Substrate Spacing	h_1	2.65398 bohr
Bond Length	h_2	2.65398 bohr
Mass	m	22032 a.u. (mass)
Friction	γ	0.02 a.u. (friction)

Table A.2: Non-Graphene Parameters used in Section 6.2

Name	**Variable**	**Value**
vdW Strength	ω	1.5655e-5 hartree
Bond Strength	k_s	3.21134e-3 a.u. (pressure)
Bending Strength	k_b	4.8e-3 hartree
vdW Radius	σ	2.53223 bohr
Substrate Spacing	h_1	2.65398 bohr
Bond Length	h_2	2.65398 bohr
Mass	m	44076 a.u. (mass)
Friction	γ	0.02 a.u. (friction)